JOURNAL OF GEOPHYSICAL RESEARCH, VOL. 114, C07017, doi:10.1029/2008JC004825, 2009

Profiles of ocean surface heating (POSH): A new model of upper ocean diurnal warming

Chelle L. Gentemann,[1,2] Peter J. Minnett,[2] and Brian Ward[3,4]

Received 24 March 2008; revised 5 March 2009; accepted 29 April 2009; published 16 July 2009.

[1] Shipboard radiometric measurements of diurnal warming at the ocean surface and profiles through the diurnal thermocline were utilized to assess the temporal and vertical variability and to develop a new physics-based model of near-surface warming. The measurements and modeled diurnal warming were compared, with the goal of comprehensively evaluating differences between the data and model results. On the basis of these results, the diurnal model was refined while attempting to maintain agreement with the measurements. Simplified bulk models commonly do not provide information on the vertical structure within the warm layer, but this new model predicts the vertical temperature profile within the diurnal thermocline using an empirically derived function dependent on wind speed. The vertical profile of temperature provides both a straightforward methodology for modeling differences due to diurnal warming between measurements made at different depths (e.g., in situ measurements at various depths and measurements of the surface temperatures by satellite radiometers) and information on upper ocean thermal structure. Additionally, the model estimates of diurnal warming at the ocean surface are important for air-sea heat and gas flux calculations, blending satellite sea surface temperature fields, and air-sea interaction studies.

Citation: Gentemann, C. L., P. J. Minnett, and B. Ward (2009), Profiles of ocean surface heating (POSH): A new model of upper ocean diurnal warming, *J. Geophys. Res.*, *114*, C07017, doi:10.1029/2008JC004825.

1. Introduction

[2] There is increasing interest in including satellite-based retrievals of sea surface temperatures (SSTs) and estimates of SST diurnal variability in the historical record for climate applications [*Kennedy et al.*, 2007; *Merchant et al.*, 2008; *O'Carroll et al.*, 2001, 2004]. Satellite data can provide much needed measurements in remote regions where the density of in situ observations is minimal. These data often lead to an improved knowledge of the spatial and temporal structure of seasonal and interannual variability and contribute to a reconstruction of global SST. Numerical Weather Prediction (NWP), climate, and mesoscale oceanography require remotely sensed SSTs with accuracy of 0.1–0.3 K [*Implementation Advisory Group*, 1999]. These applications almost always utilize daily, weekly, or monthly SST analyses derived from satellite SSTs including both nighttime and daytime SSTs. The concept of a foundation temperature, defined as SST prior to the effects of diurnal heating and cooling, was introduced by *Donlon et al.* [2001] as the ideal measurement of SST to use in the creation of accurate global SST analyses that use both daytime and nighttime measurements of SST. It is the SST most representative of the temperature of the ocean mixed layer. To determine this foundation SST, it is necessary to estimate diurnal warming at the ocean surface and remove the warming from daytime SST retrievals.

[3] Satellite measurements of SST provide a large source of data on diurnal warming, but these measurements are "snapshots" of warming, usually lacking detailed histories of radiative and surface stress forcing that are needed to understand the magnitude and temporal evolution of the diurnal heating and cooling cycle. The satellite SSTs are primarily useful because they facilitate insight by providing skin (IR) and subskin (MW) SST data and significant information on the distribution and general magnitude of warming. Geostationary satellites provide hourly measurements but calibration problems have limited their utility for diurnal studies [*Wick et al.*, 2002]. This study therefore focuses on in situ radiometric measurements of warming.

2. Background

[4] An idealized profile of upper ocean temperature is shown in Figure 1. Temperature gradients in this region affect measurements taken at different depths to differing degrees. The relationship between temperature measurements from a ship intake, usually at depths greater than 3–4 m, moored buoy observations at 1–2 m depth, drifting

[1]Remote Sensing Systems, Santa Rosa, California, USA.
[2]Rosenstiel School of Marine and Atmospheric Science, University of Miami, Miami, Florida, USA.
[3]School of Physics and Centre for Climate and Air Pollution Studies, Environmental Change Institute, National University of Ireland, Galway, Ireland.
[4]Center for Coastal Physical Oceanography, Department of Ocean, Earth, and Atmospheric Sciences, Old Dominion University, Norfolk, Virginia, USA.

0148-0227/09/2008JC004825$09.00

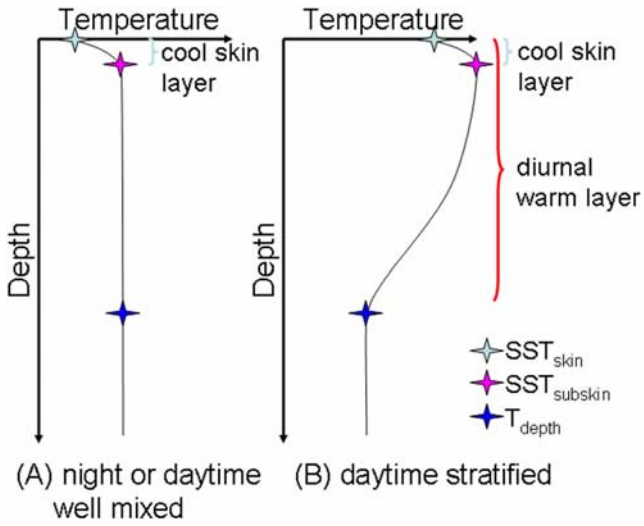

Figure 1. Idealized upper ocean temperature profile. (a) A typical nighttime profile: a well-mixed upper ocean with a cool skin layer at the air-sea interface. (b) A typical daytime profile when conditions are conducive to the formation of a diurnal thermocline. The upper ocean warms relative to the mixed layer or bulk temperature, and a cool skin layer still exists at the air-sea interface. The profile of temperature in the diurnal thermocline will depend on the absorption of radiation and whether diffusive or mechanical mixing dominates. From *Gentemann and Minnett* [2008].

buoy measurements at approximately 0.5 m or more, microwave radiometric retrievals of the upper few millimeters, and infrared radiometric retrievals of the upper submillimeter skin layer, complicate the application of these measurements in research studies.

[5] At the air-sea interface, a cool skin layer is usually present. This is a thin, thermally stratified layer that results from the upward air-sea heat flux. Within this thin, viscous layer, molecular forces dominate and molecular conduction is the primary mechanism for heat transfer. As shown in Figure 1, at the ocean surface, the cool skin layer exists both day and night [*Gentemann and Minnett*, 2008]. Below this layer, the upper ocean is often referred to as the "mixed layer" because turbulence usually produces a well-mixed layer with little stratification (Figure 1a). Yet, mixed layer is often a misnomer as stratification may be introduced either by solar warming or precipitation, for example, creating vertical temperature and density gradients (Figure 1b). Thermal stratification established by solar heating is referred to as a diurnal warm layer or diurnal thermocline. Vertical temperature gradients within the diurnal thermocline result from the varying absorption with depth (determined by the absorptivity of the water), vertical diffusion of heat, vertical stratification, and the rate of turbulent mixing. The temperature profile in the upper ocean, $T(z)$, may be defined as the summation of the cool skin, ΔT_c (z), diurnal warming, ΔT_{dw} (z), and bulk or mixed layer temperature, T_{depth},

$$T(z) = \Delta T_c(z) + \Delta T_{\mathrm{dw}}(z) + T_{\mathrm{depth}}. \quad (1)$$

[6] The temperature at the air-sea interface, $T(0)$, is well approximated by $\mathrm{SST_{skin}}$, and may then be written as the sum of diurnal warming at the surface, ΔT_{dw} (0), or ΔT_{dw}, the cool skin effect at the surface, ΔT_c (0), or ΔT_c, and the temperature at depth,

$$\mathrm{SST_{skin}} = \Delta T_c + \Delta T_{\mathrm{dw}} + T_{\mathrm{depth}}. \quad (2)$$

[7] Diurnal warming diminishes when the oceanic heat loss exceeds heat gained and the surface layer cools. The cooler, denser water near the surface results in free convection, gradually overturning a layer near the surface whose depth depends on the rate of cooling, and causing temperature gradients due to diurnal warming to diminish. Stratification also may be decreased by surface wind stress-induced mechanical mixing of the upper ocean, shear flow instabilities, breaking surface waves, or breaking internal waves.

[8] Increased daytime stratification due to diurnal warming was first reported in 1942 [*Sverdrup et al.*, 1942] and has been studied extensively since [*Defant*, 1961; *Donlon et al.*, 2002; *Fairall et al.*, 1996a; *Schluessel et al.*, 1990; *Woods and Barkmann*, 1986]. Surface temperature deviations greater than 3.0 K, referenced to subsurface temperatures below the extent of surface heating, are not uncommon and may persist for hours [*Kawai and Wada*, 2007; *Minnett*, 2003; *Yokoyama et al.*, 1995]. In section 2.1 we first present surface measurements of diurnal warming, next, previous studies investigating the upper ocean diurnal temperature profile, and, finally, present some existing diurnal variability models. Figures 1–23 and much of the discussion is presented using wind speed rather than surface stress to allow comparison between other models of diurnal heating.

2.1. Diurnal Thermocline Measurements

[9] Research on the diurnal thermocline has mostly used subsurface temperatures since these are the most commonly available measurements from buoys and ships. Determining how the diurnal variability at the ocean surface responds to variations in atmospheric forcing has been primarily addressed through theoretical modeling or extrapolation of results from in situ (buoy) measurements measured 0.5 m to 1.5 m below the skin layer [e.g., *Stuart-Menteth et al.*, 2005]. The diurnal heating signal at the ocean surface may be quite different than heating at 0.5 m as the skin layer responds very rapidly to changes in heat and momentum fluxes. After a few early publications [*Böhm et al.*, 1991; *Cornillon and Stramma*, 1985; *Deschamps and Frouin*, 1984], only recently have studies returned to examining warming at the ocean surface [*Gentemann et al.*, 2003; *Gentemann and Minnett*, 2008; *Minnett*, 2003; *Notarstefano et al.*, 2006; *Soloviev and Lukas*, 1997; *Ward et al.*, 2004a, 2004b].

2.1.1. Surface Measurements

[10] Ship-based radiometric SST measurements provide a data source for studying diurnal warming at the ocean surface. These data have a significant advantage over satellite measurements because they are usually taken from research vessels with a suite of meteorological and oceanographic instrumentation that measure many relevant parameters. They are invaluable in examining the temporal decorrelation of warming with radiative or surface stress forcing, but the limited sampling must be carefully considered.

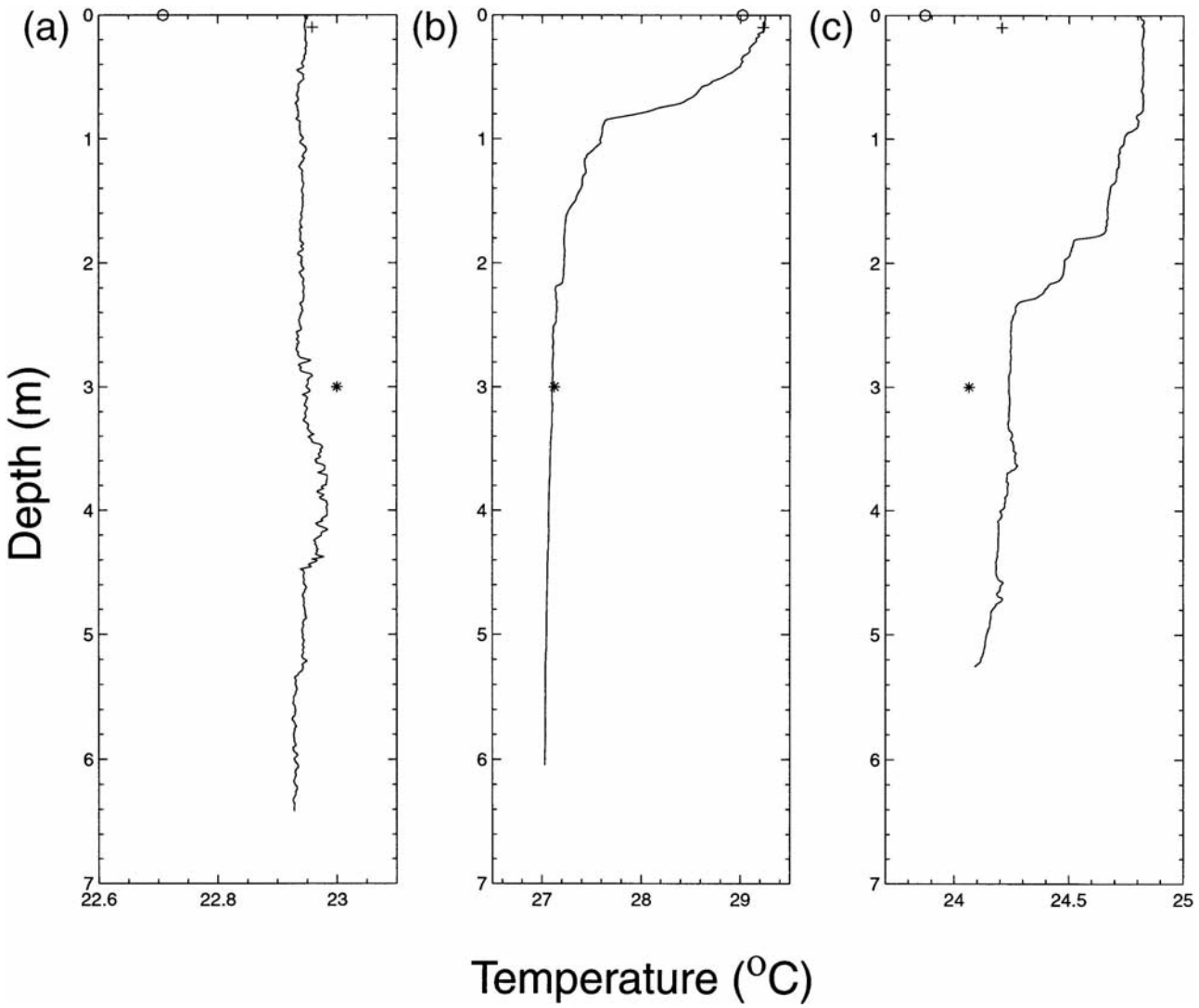

Figure 2. Vertical temperature profiles from SkinDeEP. Nearby M-AERI skin temperatures are shown by circles. A subskin temperature (at about 5 cm and close to the M-AERI field of view at the sea surface) is shown by the crosses, and the asterisks are the 3 m temperature taken by a thermosalinograph at the ship's intake, also close to the M-AERI field of view. Profiles are for different times of the day: (a) 0655 LT, (b) 1309 LT, and (c) 1920 LT. From *Donlon et al.* [2002]. Copyright 2002 American Meteorological Society (AMS).

[11] The Marine-Atmospheric Emitted Radiance Interferometer (M-AERI) [*Minnett et al.*, 2001] is a seagoing modified AERI originally developed for the Department of Energy Atmospheric Radiation Measurement (ARM) program [*Knuteson et al.*, 2004a, 2004b]. The instrument detectors receive radiation reflected by a scan mirror which views sky, sea surface, and internal calibration reference blackbodies which are traceable to National Institute of Standards and Technology (NIST) standards [*Rice et al.*, 2003, 2004]. SST is retrieved using sea and sky view data at 7.7 μm [*Minnett et al.*, 2001]. The instrument enters a safe mode during rain to avoid contamination of the scan mirror. Data from four research cruises and the cruise ship *Explorer of the Seas* provide 72 days with clear examples of diurnal warming. These days were carefully examined to ensure that the "warming" wasn't simply an artifact due to the ship

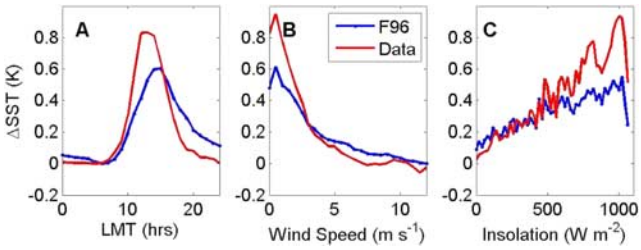

Figure 3. Diurnal amplitudes averaged over all 72 days with warming for M-AERI-derived subskin diurnal warming and two diurnal models. (a) Diurnal amplitudes as a function of LMT. (b) Diurnal amplitudes as a function of wind speed. (c) Diurnal amplitudes as a function of insolation.

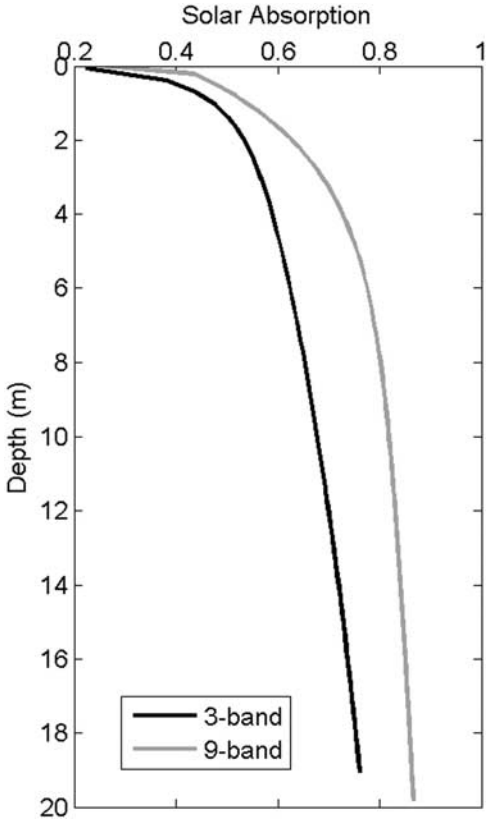

Figure 4. Three-band and nine-band absorption models for the Sun overhead.

motion (e.g., the passage through an SST front). On the research vessels, the location of the bulk SST measurements and the M-AERI observing footprint were quite close to each other, and differences due to horizontal temperature variability were not an issue. On the *Explorer of the Seas* (a much larger ship), the intake is about 15 m aft of the bow of the vessel while the M-AERI footprint was about 60 m further aft, but given the 90 s integration times of the sea view M-AERI measurements and the vessel's cruising speed through the water of 10 m s^{-1}, or more, the effects of frontal passages were not found to be a problem. Using these data, the surface diurnal warming was determined using the following methodology.

[12] From [2], the diurnal warming at the ocean surface may be defined as

$$\Delta T_{\mathrm{dw}} = T_{\mathrm{skin}} - \Delta T_c - T_{\mathrm{depth}}, \tag{3}$$

where T_{skin} is measured by M-AERI, the cool skin magnitude is estimated using *Donlon et al.*'s [2002] parameterization, and bulk temperature is measured at approximately 3 m depth by a thermosalinograph measuring the ship seawater intake. Time dependence is implicit in all terms of equation (3). A full description of the data sets and the methodology for isolating diurnal variability from the cool skin layer and other effects is given by *Gentemann and Minnett* [2008].

[13] As detailed in that paper, results are as follows: (1) the surface signature of diurnal warming is primarily related to wind speed and secondarily related to insolation;

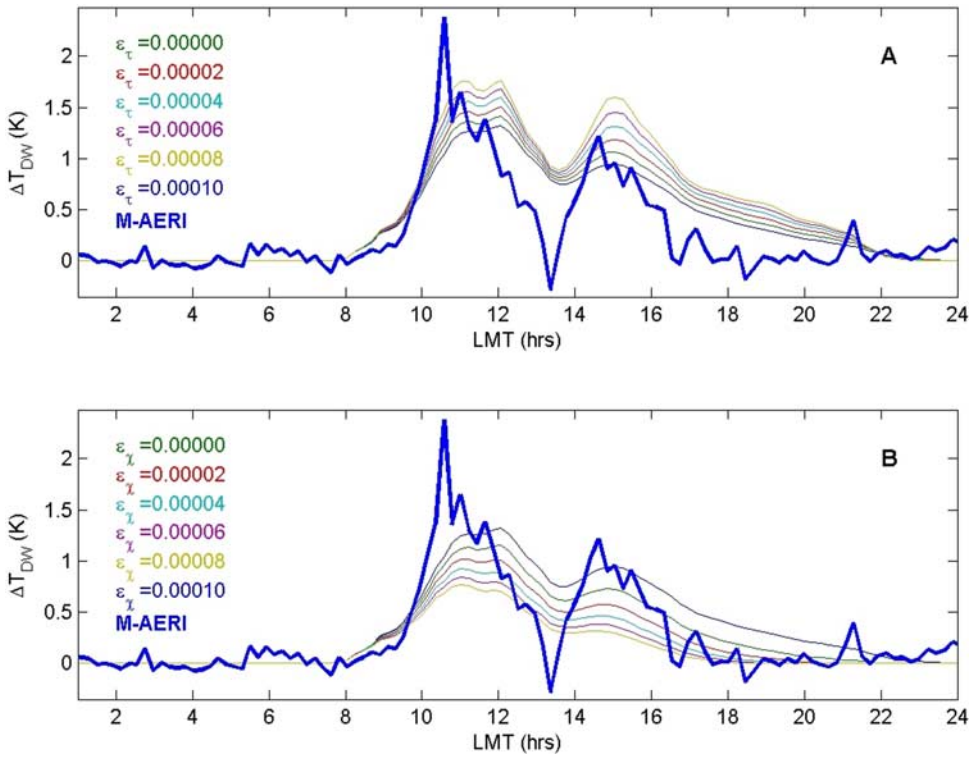

Figure 5. Testing the diminished heat and momentum in the paper by F96. (a) No dissipation in heat and increasing dissipation in wind energy. As the reduction rate increases, accumulated momentum decreases and the warming increases. (b) No dissipation in wind energy and increasing reduction of heat in the warm layer. As heat is reduced, the warming decreases.

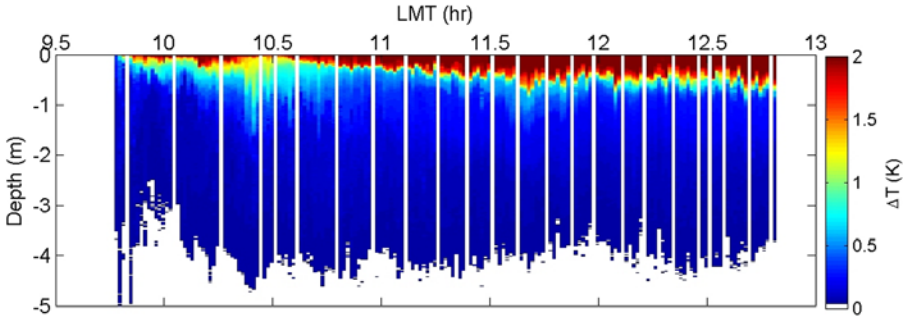

Figure 6. SkinDeEP measurements of the upper ocean diurnal thermocline on 10 October 1999. The *x* axis is local time, and each vertical colored line represents one profile taken as the profiler ascends to the surface. Profiles are repeated every 60 s. The white lines indicate missing data due to interruptions in the sequence. The colors show temperatures relative to the mixed layer temperature.

(2) small changes in wind speed (less than 1.0 m s^{-1}) rapidly and strongly affect the amplitude of diurnal warming present at the ocean surface; (3) that on the majority of days, the diurnal peak was not coincident with the insolation peak but instead directly related to the minimum wind speed during the day; and (4) that fluctuations in wind speed could result in multiple local peaks in diurnal heating in a given day. These surface measurements are valuable, but do not provide information on the vertical structure of diurnal variability. Several research cruises have been used to investigate this topic.

2.1.2. Profile Measurements

[14] A number of studies have shown an exponential decrease in temperature with depth in the diurnal thermocline. Several of these studies are detailed in Appendix A. A more recent study also examined the profile of upper ocean temperature within the diurnal thermocline using the Skin Depth Experimental Profiler (SkinDeEP) [*Ward et al.*, 2004b]. The SkinDeEP instrument was designed to measure the fine-scale thermal structure of the upper ocean. This is accomplished by descending to a depth of approximately 8 m, changing the buoyancy of the instrument by inflating a small bladder, and then ascending passively through the surface layer at about 1 m s^{-1}. As the instrument ascends, a thermistor located at the top of the instrument makes measurements. Profiles were generally taken every 60 s. While state-of-the-art instruments such as SkinDeEP are able to provide more detail about the vertical structure than moored buoys with arrays of thermometers at discrete depths, neither type of measurement provides an understanding as to why the observation is changing or information on the horizontal structure of turbulent mixing.

[15] Figure 2 [from *Donlon et al.*, 2002] shows temperature profiles taken in the Gulf of California, during October 1999. Figures 2a, 2b, and 2c have three additional temperatures, a skin temperature (circles), a subskin (0.1 m depth) temperature (crosses), and bulk (3 m depth) temperature (asterisks). The skin temperature ranges from approximately 0.2 K to 0.3 K cooler than the subskin temperature. Profiles were taken at 0655 (Figure 2a), 1309 (Figure 2b), and 1720 (Figure 2c) local time. Although wind speed was not given, Figures 2b and 2c show an approximately exponential decrease in temperature with depth. Additionally, Figure 2b reveals the importance of using a subskin SST rather than a skin or bulk SST to accurately model diurnal warming at the surface.

[16] The measurements shown above and those in Appendix A all suggest an exponential profile of tempera-

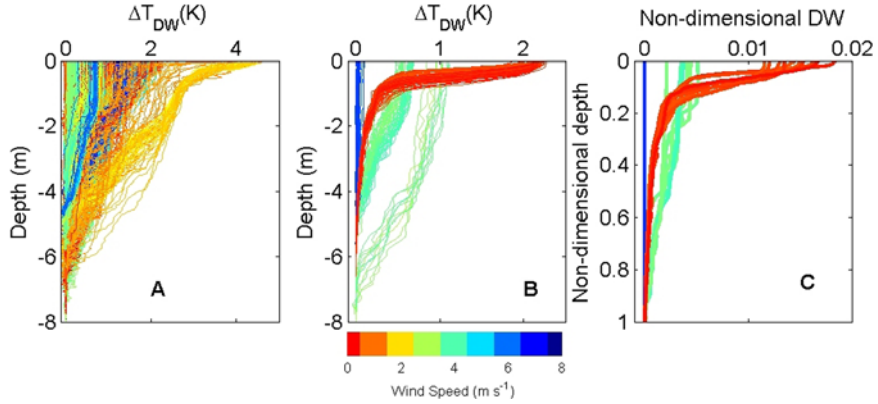

Figure 7. Upper ocean temperature profiles from SkinDeEP. The color of the lines indicates the measured wind speed at the time of the profile. (a) SkinDeEP profiles from 4 to 14 October 1999. (b) Smoothed SkinDeEP profiles from 1200 to 1400 LMT on 4 October and 8–10 October 1999. (c) The profiles from Figure 7b but with the depth normalized by the warm layer depth and normalized heat content. DW, diurnal warming.

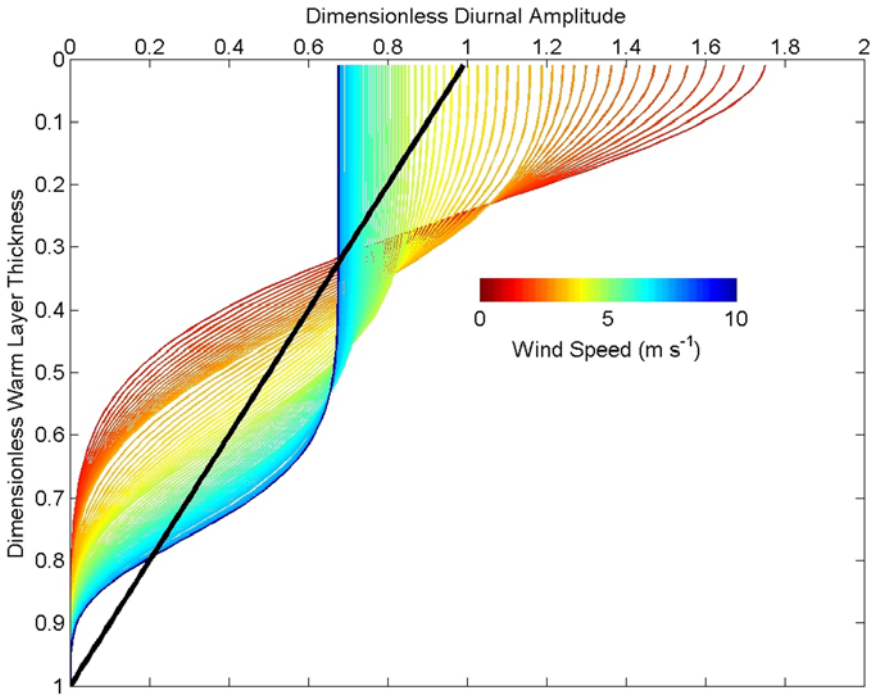

Figure 8. Analytically prescribed, normalized, diurnal warming profiles within POSH, shown by the colored lines. The linear assumption of F96 is shown by the black line.

ture with depth at very low wind speeds when there is little mechanical mixing of the ocean and the heat is trapped close to the surface, a decrease in slope of the temperature at midrange wind speeds (3.0–7.0 m s^{-1}) where some wind-induced mixing deepens the warm layer, and then a smooth transition to a well-mixed layer at higher wind speeds.

2.2. Modeling

[17] There are three common types of diurnal models: empirical, bulk, and turbulence closure. Empirical models are developed from model simulations or data analysis of measurements. These models estimate diurnal warming at a specific depth from other measurements, usually surface wind speed and insolation. This class of model has been developed to address the reality that many of the input parameters necessary to evaluate the physical models are not always available. Early empirical models depended on daily mean input parameters (usually wind and insolation) and calculated the daily maximum warming. Recently developed empirical diurnal warming models attempt to resolve intraday variability by using instantaneous or temporal averages of input parameters. The empirical models only predict warming at the surface, and only two models provide estimates of intraday variability of warming, and only one attempts to include the effects of wind and insolation history. We are not aware of any prior comparison of the empirical models or validation of the empirical models at the ocean surface using surface-based skin SST measurements.

[18] Bulk models are models of the mixed layer, where surface heat and momentum fluxes are distributed over the depth of the mixed layer. These models have been extensively tested and compared to in situ measurements under light to moderate wind conditions [*Anderson et al.*, 1996; *Cronin and McPhaden*, 1997; *Fairall et al.*, 1996a; *Shinoda and Hendon*, 1998; *Webster et al.*, 1996; *Weller and*

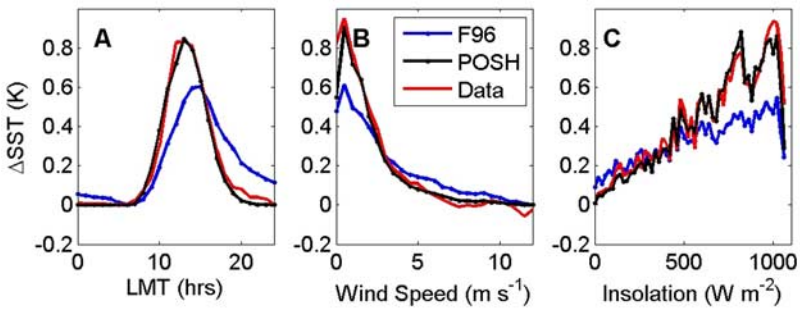

Figure 9. Diurnal amplitudes averaged over all 72 days with warming for M-AERI-derived subskin diurnal warming and the F96 and POSH diurnal models. (a) Diurnal amplitudes as a function of LMT. (b) Diurnal amplitudes as a function of wind speed. (c) Diurnal amplitudes as a function of insolation.

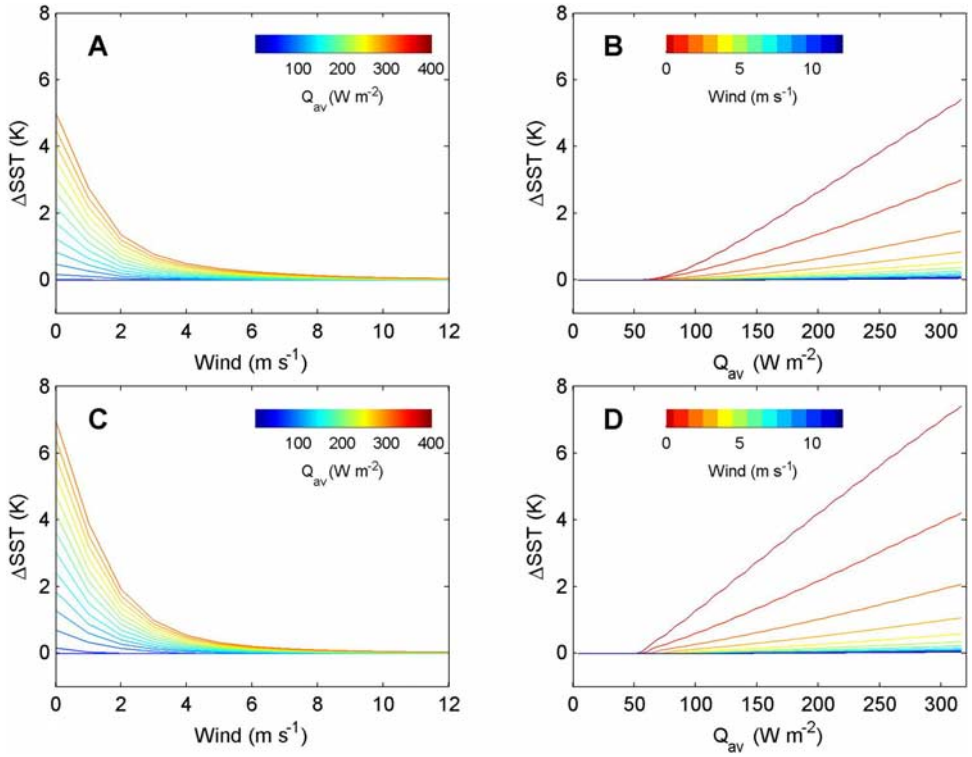

Figure 10. Sensitivity study of the (a, b) F96- and (c, d) POSH-modeled diurnal warming. Each simulation was performed with a realistically shaped 12 h day length insolation and constant wind speed.

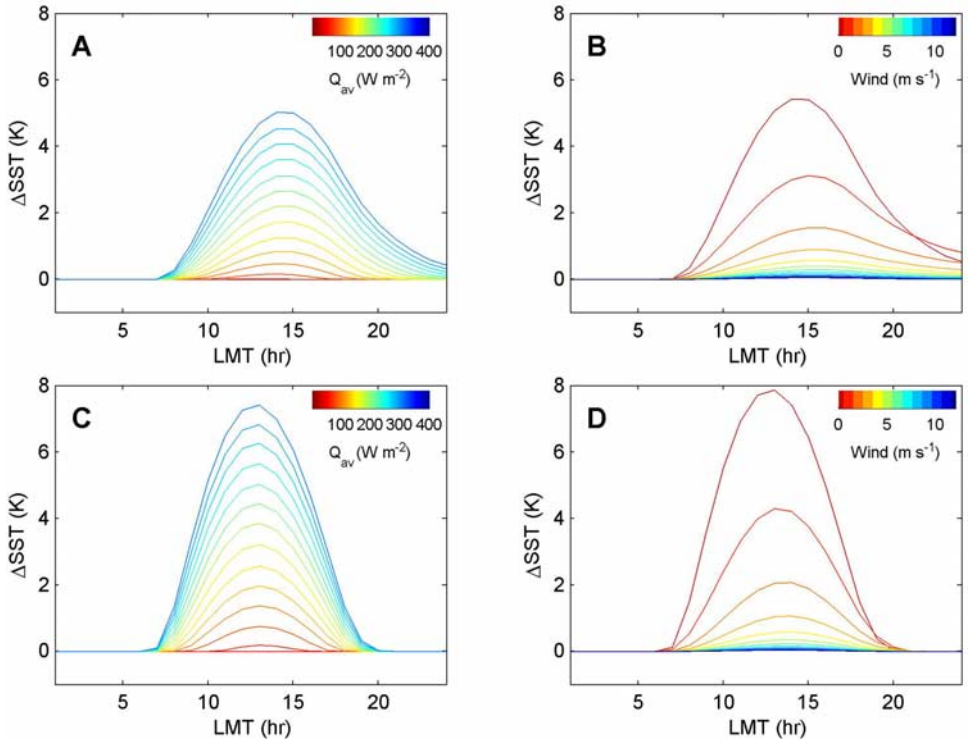

Figure 11. Simulated warming from the (a, b) F96 and (c, d) POSH models as a function of time of day. Figures 11a and 11c were evaluated with wind speed equal to 1.0 m s^{-1}, variable insolation, and length of day. Figures 11b and 11d were evaluated with daily average insolation equal to 320 W m^{-2}, variable wind speed, and length of day.

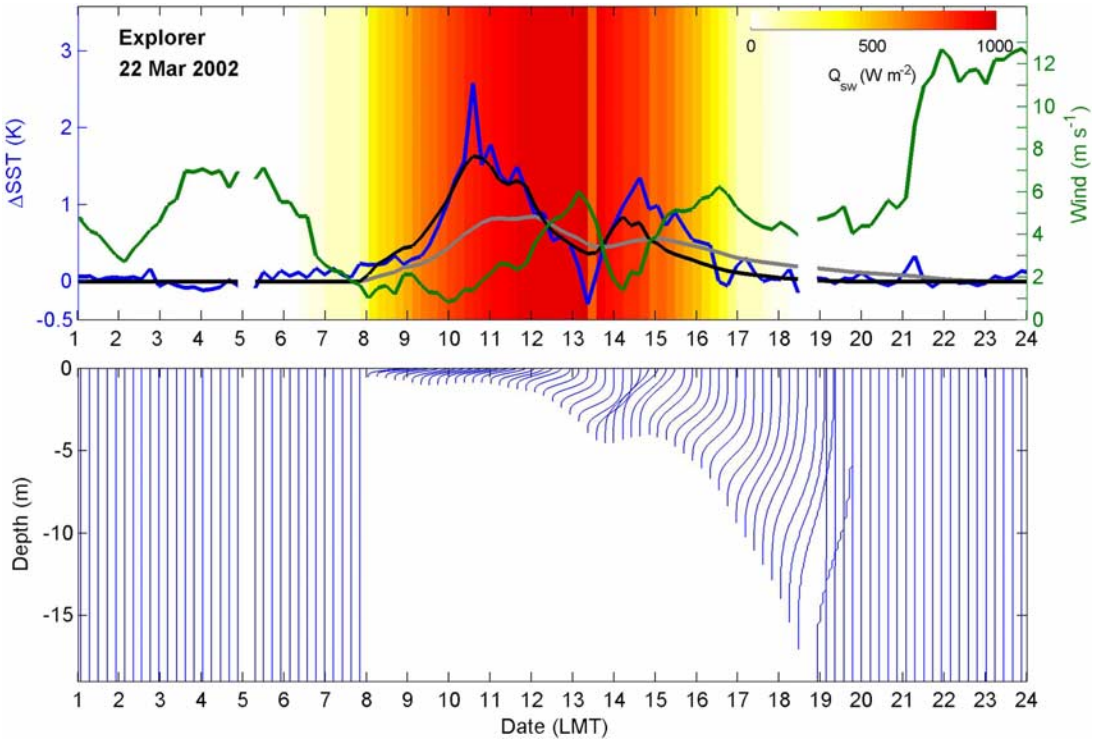

Figure 12. Two local diurnal temperature peaks in 1 single day. (top) Insolation is shown in the background, wind speed is shown by the green line (right axis), diurnal warming is shown by the blue line (left axis), F96 simulations are shown by the gray line, and POSH simulations are shown by the black line. (bottom) The POSH-modeled profiles of the temperature through the diurnal thermocline. The format is identical in Figures 12–17.

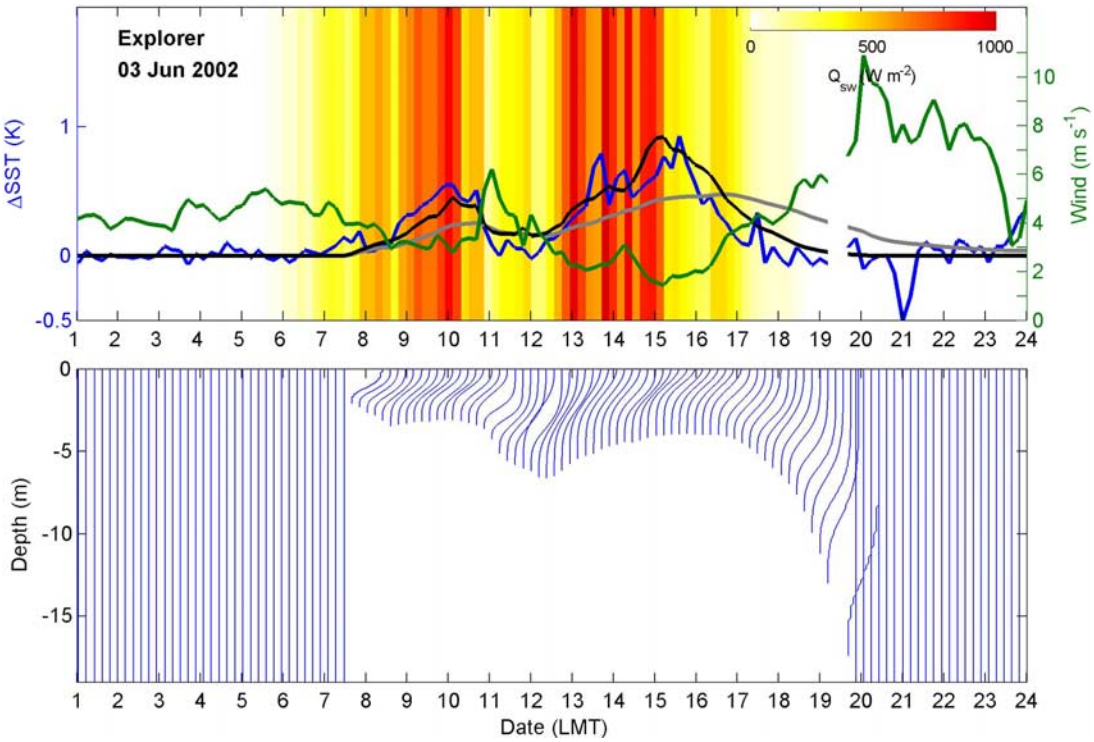

Figure 13. As Figure 12 but with variable cloud cover and two local diurnal temperature peaks.

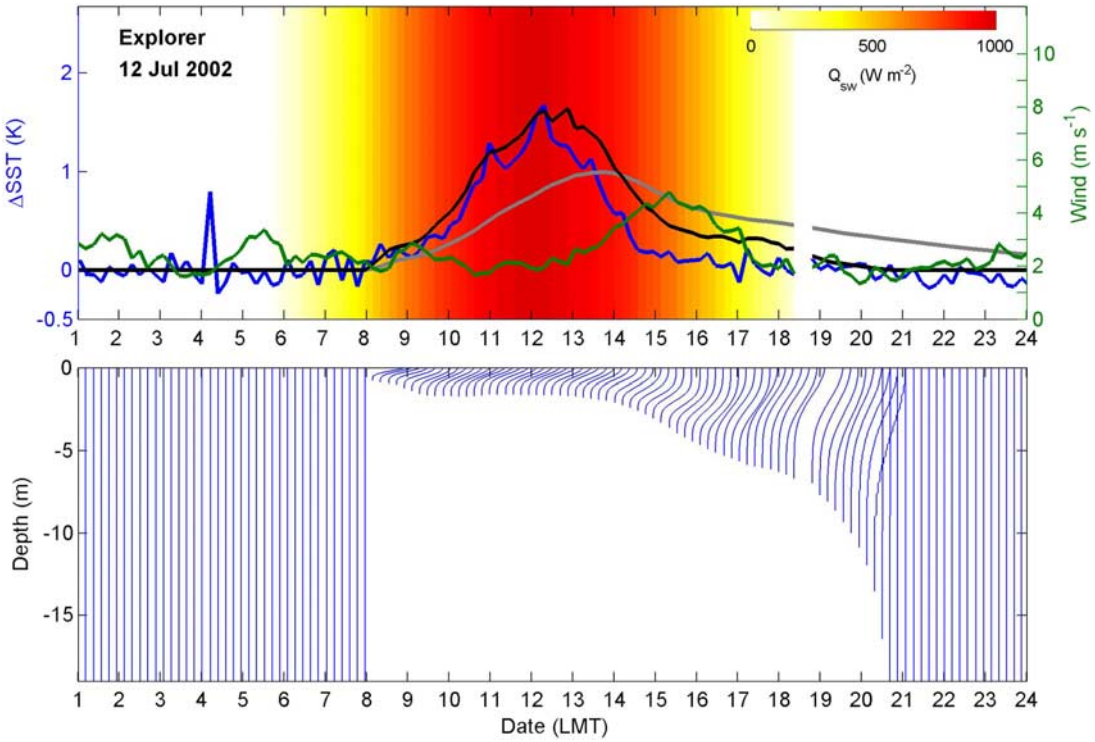

Figure 14. As Figure 12 but with a late afternoon increase in wind speed.

Anderson, 1996]. This class of model is more complicated than a simple empirical model, but depends for success on the accuracies of the parameterizations of mixing and surface fluxes and does not provide any estimates of vertical temperature structure in the upper layer.

[19] Vertical structure in the mixed layer can be determined by turbulence closure models such as those of *Mellor and Yamada* [1982] and *Kantha and Clayson* [1994]. These models find solutions to 1-D differential equations for momentum, heat, and salt by estimating turbulent fluxes

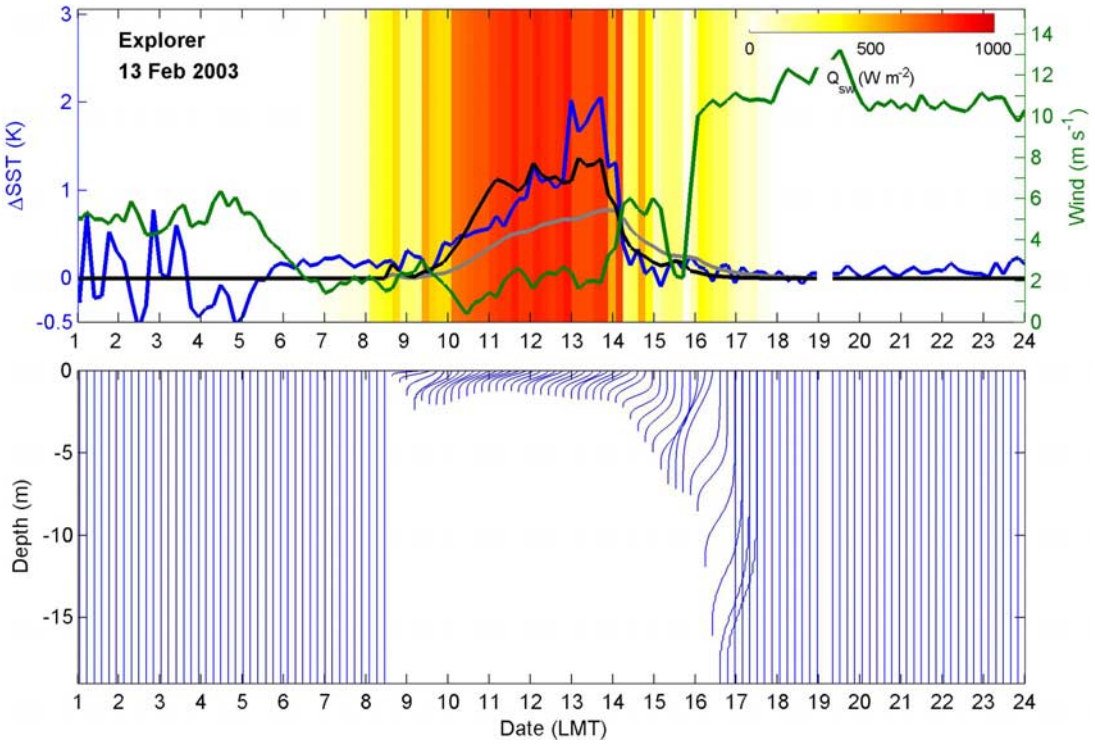

Figure 15. As Figure 12 but with an abrupt increase in wind speed.

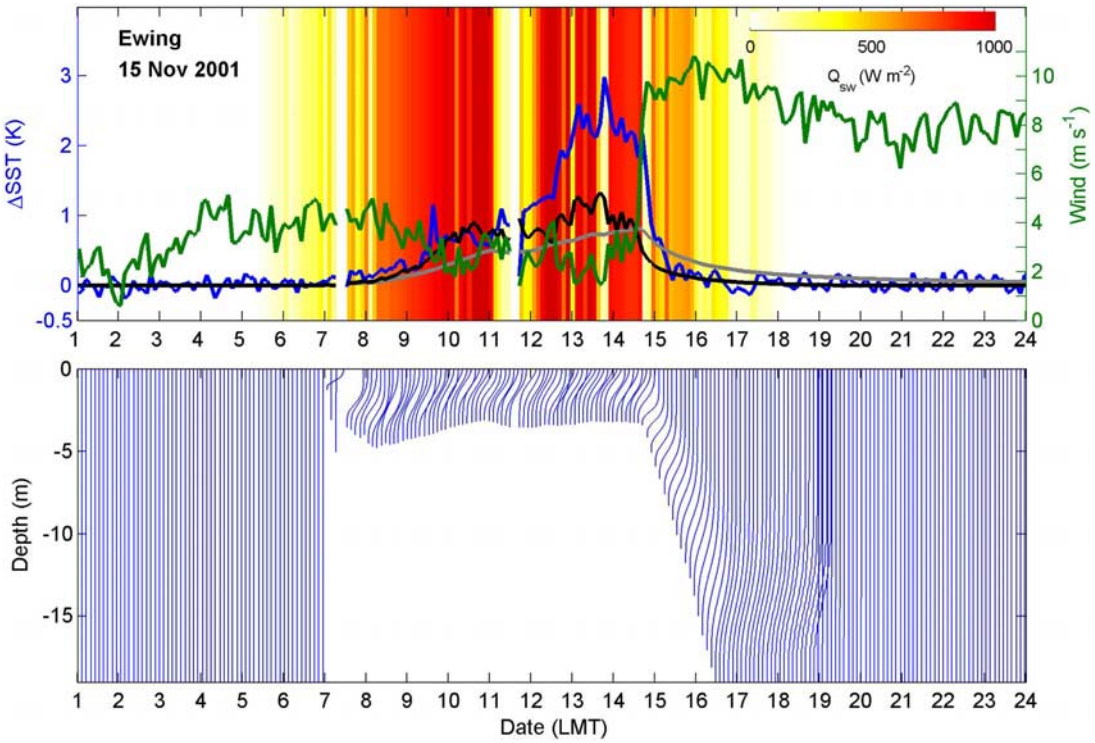

Figure 16. As Figure 12 but with a sharp increase in wind speed.

of these properties. These models are computationally intensive, dependent on mixing parameterizations, and therefore not feasible on a global scale.

[20] The research reported here aims to improve an established bulk model through better physical parameterizations determined through comparison with ship-based measurements and develop a methodology for providing turbulence closure–like vertical structure within the warm layer.

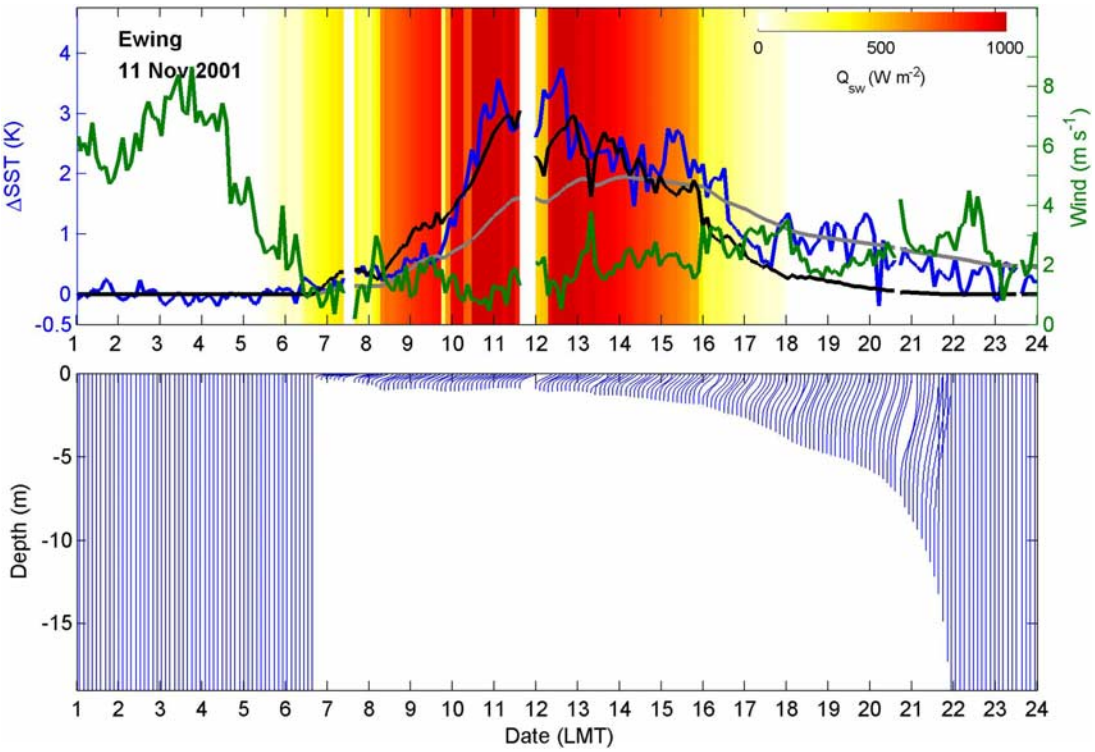

Figure 17. As Figure 12 but with an early peak in warming.

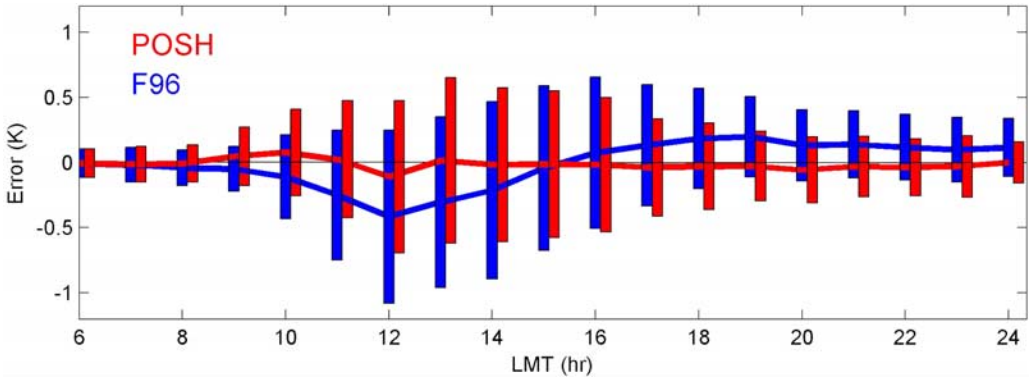

Figure 18. Hourly bias and standard deviation for the POSH and F96 models compared to the in situ data. The bias is plotted as the solid line, and the standard deviation is given as the vertical bars. The POSH bias is always less than the F96 bias, and the POSH standard deviation is less for all LMT hours except 0900.

2.3. *Fairall et al.*'s [1996a] Model

[21] *Fairall et al.*'s [1996a] (hereinafter referred to as F96) diurnal heating model is based on *Price et al.*'s [1986] (hereinafter referred to as PWP) model which, in turn, has its heritage in the dynamical instability model of *Price et al.* [1978]. The one-dimensional bulk model assumes that the diurnal layer is noninteractive with the mixed layer and assumes that the mixed layer is well mixed with very small vertical gradients. The model determines the diurnal warming as the summation of vertical mixing and radiation processes driven solely by local surface heat and momentum fluxes [*Niiler and Kraus*, 1977]. Surface values are assumed to be known, as the surface flux is equal to the net heat flux, the freshwater flux is equated to the difference between evaporation and precipitation, and the surface stress is entirely wind driven. The model used in this analysis (bulk flux version 2.5b) is code developed by Tropical Ocean–Global Atmosphere (TOGA) Coupled Ocean-Atmospheric Response Experiment (COARE) investigators. The TOGA COARE flux algorithm is now up to version 3.0 [*Fairall et al.*, 2003]. The only differences between these versions that may affect these results are small changes to the calculation of the latent heat flux. The representation of the warm layer was not changed in the new version.

[22] The net heating within the warm layer is the difference between the solar insolation absorption within the warm layer and the total heat loss at the surface. The F96 version simplifies the PWP model by making the assumption that there is a linear gradient in temperature through the warm layer, which will always satisfy the PWP criterion for static stability. The model also requires mixed layer stability but does not require the shear flow stability. F96 determined the diurnal heating at the surface, T_w, as

$$T_w = \frac{2Q_{ac}}{\rho c_p D_T}, \tag{4}$$

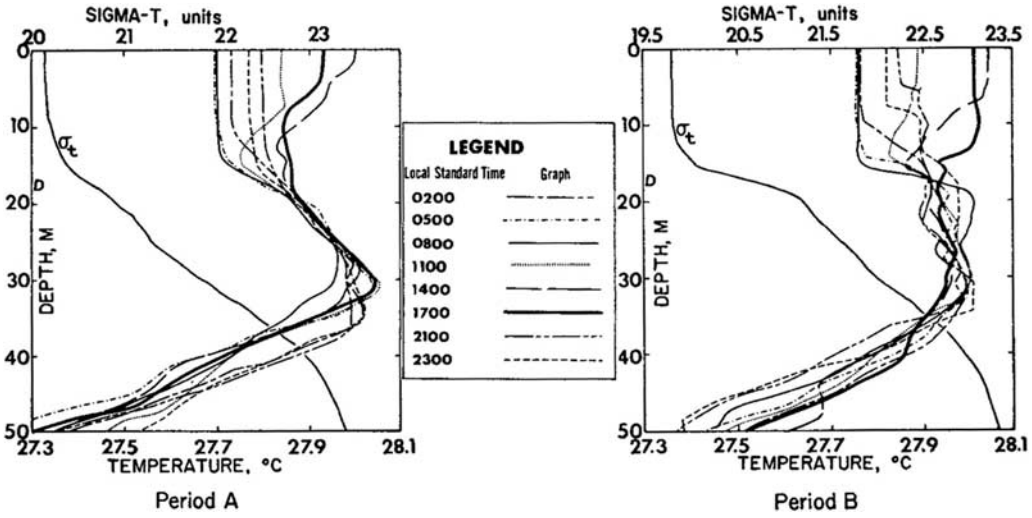

Figure 19. Diurnal temperature profiles and sigma-T profiles for the R/V *Discoverer*. The depth of minimum temporal change in heat content is indicated by the letter D. From *Delnore* [1972]. Copyright 1972 AMS.

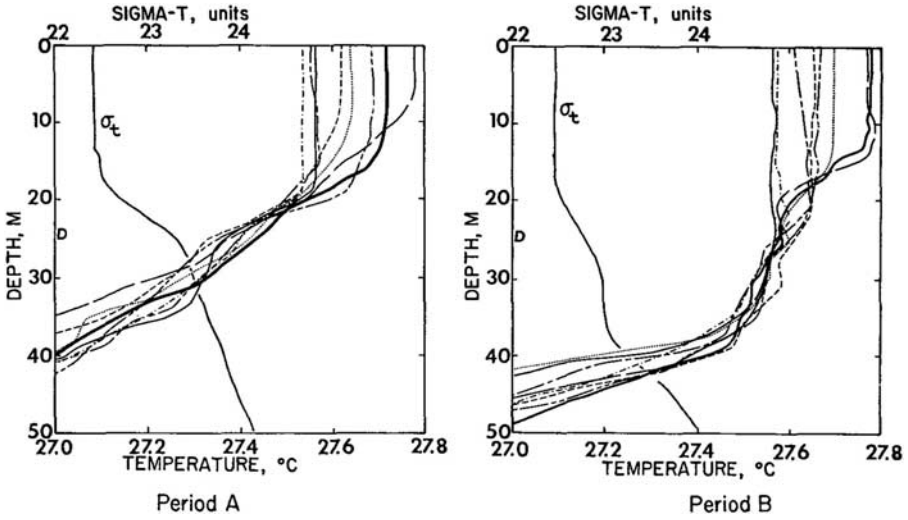

Figure 20. Same as Figure 19 but for the R/V *Oceanographer*. From *Delnore* [1972]. Copyright 1972 AMS.

where ρ is the density, c_p is the specific heat at constant pressure, warming is confined to a depth, D_T, and the integrated radiative fluxes, Q_{ac}, at each time step Δt, are

$$Q_{ac}(t) = Q_{ac}(t - \Delta t) + Q_{\text{tot}}\Delta t, \tag{5}$$

where Q_{tot} is the net heat flux. D_T is determined by requiring the bulk Richardson number, R_i, to be equal to 0.65 [*Fairall et al.*, 1996a],

$$D_T = \sqrt{\frac{2R_i c_p}{\alpha g \rho}} \frac{\tau_{ac}}{\sqrt{Q_{ac}}}, \tag{6}$$

where α is the thermal expansion coefficient, g is the acceleration due to gravity, and the integrated wind stress, τ_{ac}, is

$$\tau_{ac}(t) = \tau_{ac}(t - \Delta t) + \tau_{\text{tot}}\Delta t, \tag{7}$$

and surface stress is

$$\tau_{\text{tot}} = \rho_a u_*^2, \tag{8}$$

where ρ_a is the density of air and u_* is the friction velocity.

[23] The net heat flux within the warm layer is

$$Q_{\text{tot}} = Q_{\text{SW}} f_w(D_T) - (Q_{\text{LW}} + Q_{\text{sens}} + Q_{\text{lat}} + Q_{\text{rain}}), \tag{9}$$

where the heat flux due to rain, Q_{rain}, which here is set to zero since the available at-sea measurements do not include

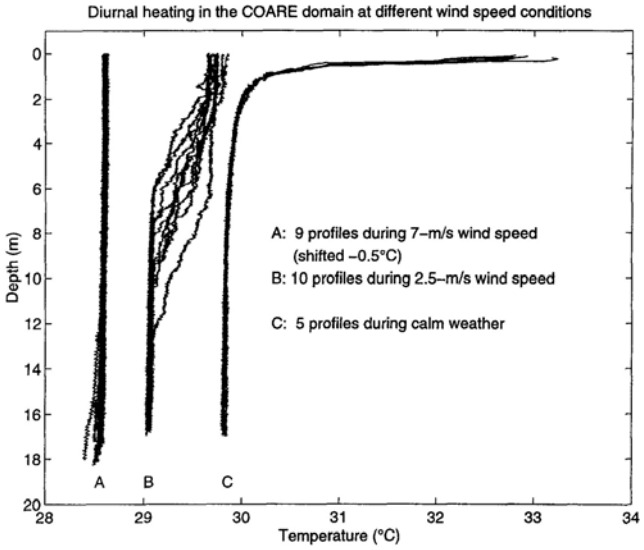

Figure 21. Lines A, B, and C show vertical temperature profiles in near-surface layer of the ocean in the TOGA COARE domain obtained by free-rising profiler at different wind speeds in the afternoon. Reprinted from *Soloviev and Lukas* [1997]. Copyright 1997 with permission from Elsevier.

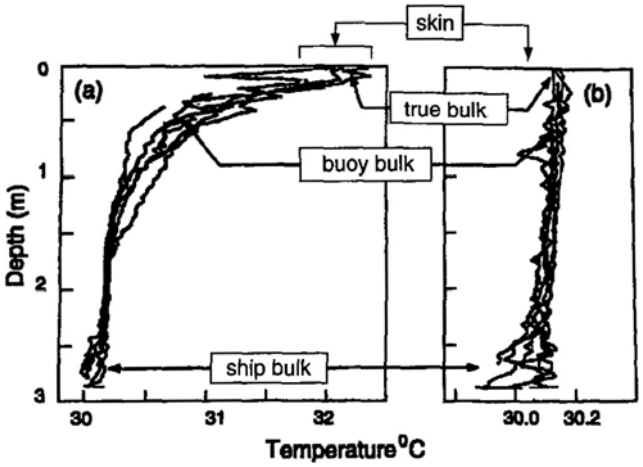

Figure 22. Measurements of temperature profiles in the ocean mixed layer on (a) 13 January 1993 and (b) 4 February 1993. The levels where the skin, true bulk, buoy bulk, and ship bulk SST values are commonly measured are indicated schematically. From *Webster et al.* [1996]. Copyright 1996 AMS.

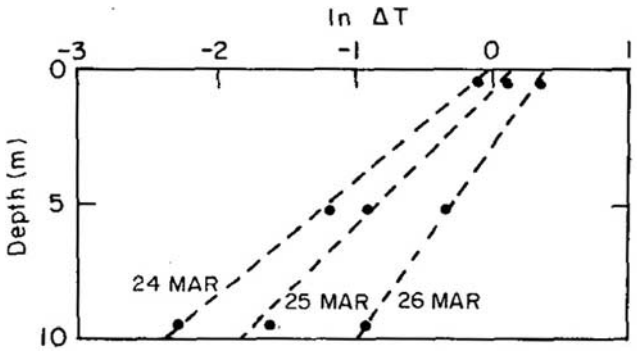

Figure 23. Semilog plot of the diurnal temperature range (ΔT) versus depth on 24–26 March 1974. Prepared from hourly averages of the thermistor data. From *Halpern and Reed* [1976]. Copyright 1976 AMS.

rain events. f_w (D_T), is the attenuation of shortwave radiation within the warm layer, Q_{SW} is the net shortwave radiation, Q_{lat} is the latent heat flux, Q_{sens} is the sensible heat flux, and Q_{LW} is the net longwave radiation,

$$Q_{LW} = \varepsilon_{LW}\left(\sigma_{SB} T_{skin}^4 - Q_{LW\downarrow}\right), \tag{10}$$

where ε_{LW} is 0.97, the mean emissivity of the sea surface for longwave radiation and σ_{SB} is Stephen-Boltzman constant, 5.67×10^{-8} W m^{-2} K^{-4}. T_{skin}, and downwelling longwave, $Q_{LW\downarrow}$, are assumed to be known. Shortwave (solar) insolation is

$$Q_{SW} = (1 - r_{SW}) Q_{SW\downarrow}, \tag{11}$$

where, r_{SW}, the mean reflectivity of the sea surface for shortwave radiation is 0.055 [*Fairall et al.*, 1996b], and the shortwave radiation, $Q_{SW\downarrow}$, is assumed to be known. Within the warm layer, the solar radiation is absorbed at depth using a three-band exponential model of absorption:

Q_{sens} and Q_{lat} are

$$Q_{sens} = \rho_A C_H u (T_{skin} - T_a) \tag{12}$$

$$Q_{lat} = \rho_a C_E u (q_S - q_A), \tag{13}$$

where C_H is the bulk transfer coefficient (Stanton number) for sensible heat, C_E is the bulk transfer coefficient for latent heat (Dalton number), u is wind speed at 10 m, T_a is the air temperature at 10 m, q_S is the saturation specific humidity at the surface, and q_A is the specific humidity of the air at 10 m.

3. Development of the New Diurnal Model, Profiles of Surface Heating

3.1. Background

[24] Simulations from the F96 model were compared to the subskin diurnal warming derived from M-AERI revealing significant differences. As discussed above, the F96 model development, and previous validation studies, have mostly utilized measurements below the subskin layer, at depths of 0.5 m and greater. Temperature at these depths has a very different response to surface heat and momentum fluxes than the surface layer. The comparisons to subskin diurnal warming measurements led to the development of a new model based on the F96 model. The refinements and then the comparisons to M-AERI data are discussed in section 3.2. The model refinements were mostly based on the average diurnal warming for 72 days that were identified as having a clear diurnal warming signal (Figure 3). These data are discussed in more detail by *Gentemann and Minnett* [2008]. The key differences when the observed diurnal warming was compared to the F96 simulations were F96 underestimated the amplitude of warming (Figure 3a), the peak in modeled warming occurred after the peak in data, modeled warming persisted beyond observed warming in the afternoon; modeled warming underestimated amplitudes at low wind speeds and overestimated at high wind speeds (Figure 3b), and modeled warming was underestimated at high insolation (Figure 3c). These are the key aspects the new model addresses. Improvements to the mean simulations for individual days were expected from this methodology, but improvements in the standard deviation of the difference between simulations and data were not guaranteed.

3.2. Refinements Applied to F96

[25] The F96 model was refined here in several ways to improve simulations of the observed diurnal warming at the surface. The first modification to the model was to change the setting to zero of accumulated heat and momentum from 0000 to 0600 local mean time (LMT). The F96 model includes no dissipation and so rapidly diverges from measurements because of the lack of viscous dissipation as well as any exchange of heat or momentum through the base of the warm layer. Accumulated momentum, heat, and diurnal warming were all set to zero at 0000 by F96. However, warming may be present through the night and into the next day when wind speeds are low and the diurnal thermocline is not entirely eroded. While this situation certainly occurs, the study presented here, focuses on the warming within 1 single day, and it is therefore appropriate to set the model to zero at 0600 LMT. Additionally, although persistent thermoclines develop, especially in the tropics [*Katsaros et al.*, 2005], diurnal thermoclines still develop near the surface within these regions.

[26] The parameterization of solar absorption within the F96 model was changed from a three-band spectral parameterization to one with nine bands (Figure 4), developed by *Paulson and Simpson* [1981]. The nine-band model has stronger absorption at all depths, but particularly at shallow layers and thus should better capture the heating profile for shallow diurnal thermoclines. The effect of the subsurface solar angle, θ, was also included to better model the depth of radiation absorption:

$$\begin{aligned} f_w(z,\theta) = 1 - \Big(&0.2370 e^{\frac{-z\cos(\theta)}{34.840}} + 0.36 e^{\frac{-z\cos(\theta)}{2.266}} + 0.1790 e^{\frac{-z\cos(\theta)}{0.0315}} \\ &+ 0.0870 e^{\frac{-z\cos(\theta)}{0.0055}} + 0.0800 e^{\frac{-z\cos(\theta)}{8.32\times10^{-4}}} + 0.025 e^{\frac{-z\cos(\theta)}{1.26\times10^{-4}}} \\ &+ 0.0250 e^{\frac{-z\cos(\theta)}{3.13\times10^{-4}}} + 0.007 e^{\frac{-z\cos(\theta)}{7.82\times10^{-4}}} + 0.0004 e^{\frac{-z\cos(\theta)}{1.44\times10^{-5}}}\Big). \end{aligned} \tag{14}$$

[27] This new spectral absorption model slightly improved the skill of the model at lower wind speeds (when compared to M-AERI data) by increasing the simulated warming. The change in the absorption model did not make a significant difference because the model only considers radiative forcing to the base of the diurnal thermocline, and this is often fairly shallow (less than 5 m) when wind mixing is small enough to allow the formation of a diurnal thermocline. Simulated warming was still low when compared to the M-AERI measurements; therefore the nine-band spectral absorption model was increased by 20%, for all wind speeds, determined by comparing the ship-based measured diurnal amplitudes to the original model predictions. The nine-band model was developed using clear water and has been found to underestimate absorption in the ocean. *Soloviev and Schlüssel* [1996] proposed modified irradiance absorption coefficients, for the 0.2–0.6 μm wavelength in the nine-band model, on the basis of Jerlov water classification. According to this model, a Jerlov II water increases absorption by approximately 12% while a Jerlov III increases it by approximately 20%. The regions of this study are mostly Jerlov I or II type waters, but using absorption coefficients appropriate for these conditions led to consistent underestimation of the warming, so we chose to increase absorption by 20%, but the model does not explicitly depend on Jerlov classification type. The total radiative forcing within the warm layer utilized in the new model is then

$$Q_{\mathrm{tot}} = 1.2 Q_{\mathrm{SW}} f_w(D_T) - (Q_{\mathrm{LW}} + Q_{\mathrm{sens}} + Q_{\mathrm{lat}}). \qquad (15)$$

[28] While this increased the warming amplitudes slightly, this change did not affect warming still present in the F96 model well beyond that observed in the late afternoon and evening (Figure 3a). This was a result of the accumulated warm layer heat only decreasing through longwave radiation and turbulent surface fluxes. The warm layer was assumed to be "cut off" from the mixed layer. In reality, the heat content will be diminished through conduction and turbulent mixing across the base of the warm layer (entrainment). Additionally, momentum will dissipate through viscous effects and diminish through entrainment. Using these arguments, both momentum and heat content were reduced. The original model accumulates wind stress, momentum, and heat by adding wind stress, τ, and total heat flux, Q, from the previous time step, determined by the data, and usually 8–12 min, equations (5) and (7). Thus,

$$\tau_{\mathrm{ac}}(t) = (1 - \varepsilon_\tau \Delta t)\tau_{\mathrm{ac}}(t - \Delta t) + \tau_{\mathrm{tot}} \Delta t \text{ and}$$

$$Q_{\mathrm{ac}}(t) = \left(1 - \varepsilon_\chi \Delta t\right) Q_{\mathrm{ac}}(t - \Delta t) + Q_{\mathrm{tot}} \Delta t, \qquad (16)$$

$$\text{where } \varepsilon_\tau = 0.00005 \text{ s}^{-1}; \varepsilon_\chi = 0.00008 \text{ s}^{-1}.$$

[29] All 72 days of diurnal warming measurements were run with variable ε_τ and ε_χ. The simulated warming was compared to the measured warming and the reduction rates, ε_τ and ε_χ, was determined by minimizing the standard deviation of the difference between the simulations and the data. In this model, less momentum reduces turbulent mixing in the warm layer, and this decreases the depth of the warm layer, intensifying the stratification, and thereby increases the modeled surface warming. Conversely, reduction of heat in the warm layer through exchange with the mixed layer beneath increases the depth of the warm layer and decreases the modeled surface warming (Figure 5).

[30] The model with reduced heat and momentum responded better to variations in surface stress and heat fluxes. Two measured skin SST peaks in warming (Figure 5, blue line) illustrate how, by diminishing accumulated momentum, the separate peaks are better represented. The original model, F96, resolves the first peak but does not resolve the second peak well, while the new model is more responsive and better matches the variability seen in the measurements. The reduction of heat in the warm layer reduces the late afternoon overestimation of warming simulated by the original F96 model (Figure 5b).

[31] While reducing accumulated heat and momentum improved the F96 temporal response to solar heating and shear-induced mixing, the wind speed dependence still did not match the measurements well (Figure 3b). The original model underestimated warming at low wind speeds and overestimated warming at higher winds. It was determined that the F96 assumption of a linear profile of temperature within the warm layer would cause this result. The F96 model assumes warming is a maximum at the surface and decreases linearly to zero at the base of the diurnal warm layer. Previous studies of upper ocean temperature profiles do not show a linear temperature change in the warm layer, but instead appear to approximate an exponential and then, with wind mixing, a constant mixed warm layer near the surface which then decreases at depth (e.g., see section 2.1.2 and Appendix A). At low wind speed the diurnal thermocline has minimal turbulent mixing, leading to strong stratification. For seawater with uniform optical properties in the upper layer, the profile of absorption of shortwave radiation is generally assumed to be exponential and it is therefore likely that the profile of warming has a similar shape at low wind speeds. As the wind increases, mixing in the warm layer increases, temperature gradients in the diurnal thermocline diminish until the thermocline disappears.

3.3. SkinDeEP Measurements

[32] The SkinDeEP instrument characteristics were introduced in section 2.1.2. Vertical profiles of upper ocean temperature from the SkinDeEP are shown in Figure 6. In this example, the warming is mainly confined to the upper 1–4 m of ocean. There is a short decrease in insolation near the second tick on the x axis (a cloud passed over) and the warm layer rapidly diminishes. After the cloud passes, the warm layer is rapidly reestablished. There is variability in the amount, depth, and vertical distribution of diurnal heating. Thus, while the data are highly accurate, looking at the data in isolation, it is difficult to determine exactly what is being measured: local diurnal variability, nonlocal variability (internal waves, horizontal advection), or a feature due to the sampling environment. Because of these issues, rather than make direct comparisons, in the study, we use SkinDeEP measurements to guide us in the parameterization of the wind speed dependence of the vertical structure of temperature in the diurnal thermocline.

[33] The SkinDeEP was deployed from the Scripps Institution of Oceanography (SIO) R/V *Melville* during the 1–21 October 1999 Marine Optical Characterization

Table 1. Coefficient for Equation (19)[a]

Wind Speed	a
$\leq$1.5	2
3	3
4.5	5
6	7
$\geq$7.5	9

[a]Above 1.5 m s^{-1} and below 7.5m s^{-1}, equation (19) is linearly interpolated between results.

Experiment-5 cruise. The ship left San Diego for the Gulf of California, staying briefly off of the west coast of Mexico. Profiles were collected on several days while the ship maintained station [*Ward*, 2006]. SkinDeEP profiles of temperature through the diurnal thermocline are shown in Figure 7. Figure 7a shows data from several different stations with different wind and insolation histories. The groupings of curves shown in Figure 7a are generally from different days. To examine the wind speed dependence, data from 1200 to 1400 LMT, taken at several different wind speeds but with similar insolation were examined (Figure 7b). The data clearly show different temperature gradients for different wind speeds. The warming does not consistently decrease with wind speed, likely because this is a snapshot of days with different wind and radiative fluxes. The profiles taken with wind speeds of 0–1 m s^{-1} (red lines) have an apparently exponential decay of temperature with depth. As winds increase slightly, 1–2 m s^{-1} (orange and yellow lines), mixing in the upper layer causes the profiles to be quite well mixed and have small temperature gradients in the top 0.25 m. At even higher wind speeds (green and blue lines) the profile takes on a nonexponential shape. The wind-induced mixing results in an increasingly eroded diurnal thermocline, decreasing the mean temperature gradients, so the profile becomes more isothermal.

[34] The same profiles, but normalized by warm layer depth and heat content are shown in Figure 7c. All profiles were referenced to the mixed layer temperature, taken as the mean temperature from the deepest 0.5 m in each profile, usually between 4 and 8 m depth. This assumes that the diurnal thermocline thickness is less than the profiler's maximum depth and, on most days, it is clear that this assumption is correct. The base of the diurnal thermocline in each profile is determined as the first depth where the temperature equals to the estimated mixed layer temperature. At lower wind speeds, an exponential temperature decrease with depth is observed, while higher wind speeds lead to a decreased vertical gradient near the surface that then decreases at depth to zero, indicating more mixing in the upper surface.

3.4. Development of the Profiles of Surface Heating Model

[35] Section 3.3 introduces a methodology to determine diurnal thermocline profiles on the basis of determination of warm layer depth and magnitude of the heat content. The wind speed dependence of these diurnal profiles was reproduced by equation (17), with depth normalized by the diurnal warm layer thickness and normalized heat content,

$$\Delta T(z) = e^{-9.5\left(\frac{z}{D_T}\right)^a}, \qquad (17)$$

where a is determined by the wind speed as shown in Table 1. As the wind speed changes, the new temperature profiles (Figure 8) smoothly transition between the different equations using linear interpolation. The F96 diurnal thermocline heat content is calculated using the original linear profile of F96 and its estimate of surface warming. In the new model, a profile is calculated at each time step, with the vertical axis scaled by the depth of the warm layer. The magnitude is adjusted so that the new profile and the original linear temperature gradient have the same total heat content. In this way, the total heat content is the same but the profile, and therefore surface expression of warming, is quite different. The profile scales with the warm layer depth to ensure that it smoothly decreases to zero at the base of the warm layer. This refined F96 model, with diminished momentum and heat content in the diurnal thermocline, increased solar absorption, and explicit wind speed–dependent vertical structure is referred to hereinafter as the profiles of ocean surface heating (POSH) model.

3.5. Comparisons Between F96 and POSH by Model Simulations

[36] To establish the benefits of the new model formulation, the dependence of diurnal warming on variations in wind speed, insolation, and time of day was explored for both the F96 and POSH models. The POSH model matches the surface diurnal warming data better than the F96 model (Figure 9), where the POSH model has shifted the peak warming earlier than F96 and decreased warming in the afternoon, both effects matching the measurements better (Figure 9a). POSH has increased warming at low wind speeds and decreased at high wind speeds when compared to the F96 model (Figure 9b). The dependence on insolation shown in Figure 9c is also improved on that of from the F96 model.

[37] To determine the dependence on variations in wind speed, insolation, and time of day, model simulations were evaluated using 24 h periods, during which insolation was varied realistically through the day. The length of day was kept constant for all simulations; only the amplitude of insolation decreased using a simple multiplicative factor. The 24 h model simulations were driven using daily average insolation ranging from 0 to 400 W m^{-2} at increments of 1 W m^{-2}. For each insolation factor, the model was run with different constant wind speeds through the day, varying from 0.2 m s^{-1} to 11.8 m s^{-1} at increments of 0.2 m s^{-1} (60 wind speed cases). The dependence of the subskin SST on wind speed and insolation at 1400 LMT for both the F96 and POSH models show little warming above 6 m s^{-1} and below 80 W m^{-2} (Figure 10). The maximum warming is 5.4 K (F96) and 7.4 K (POSH). The temporal dependence of F96 and POSH on local time is illustrated in Figure 11. The peak warming in the F96 model occurs at 1400 LMT, 2 h after the peak in maximum insolation. In the POSH simulations, the reduced heat in the diurnal thermocline has changed the temporal dependence to a less skewed shape that more closely resembles the actual insolation forcing, with the simulated warming peaks at 1300 LMT.

3.6. Evaluation of the Models With in Situ Data

[38] The POSH model was evaluated by examining individual days with M-AERI measurements of diurnal

Table 2. Model Performance for Individual Cruise Days[a]

			Mean (K)		STD (K)	
	Vessel	Date	F96	POSH	F96	POSH
1	Explorer	7 Sep 2001	0.01	0.01	0.17	0.20
2	Explorer	28 Sep 2001	0.10	0.14	0.23	0.18
3	Explorer	8 Feb 2002	−0.19	−0.03	0.53	0.45
4	Explorer	22 Mar 2002	−0.12	−0.06	0.37	0.22
5	Explorer	28 Mar 2002	0.00	0.02	0.26	0.18
6	Explorer	5 Apr 2002	−0.03	−0.03	0.25	0.15
7	Explorer	22 Apr 2002	−0.01	−0.04	0.16	0.15
8	Explorer	3 Jun 2002	0.01	0.03	0.22	0.14
9	Explorer	7 Jun 2002	−0.01	−0.01	0.20	0.25
10	Explorer	5 Jul 2002	−0.39	−0.23	0.61	0.39
11	Explorer	7 Jul 2002	0.06	0.09	0.23	0.17
12	Explorer	12 Jul 2002	0.13	0.15	0.37	0.16
13	Explorer	2 Aug 2002	−0.05	0.01	0.20	0.40
14	Explorer	9 Aug 2002	−0.08	−0.05	0.18	0.12
15	Explorer	25 Dec 2002	−0.17	−0.14	0.40	0.35
16	Explorer	13 Feb 2003	−0.17	−0.07	0.30	0.21
17	Explorer	21 Mar 2003	−0.25	−0.25	0.82	0.65
18	Explorer	30 Mar 2003	0.00	−0.02	0.17	0.13
19	Explorer	27 Apr 2003	0.03	0.07	0.49	0.28
20	Explorer	16 May 2003	0.04	0.08	0.21	0.16
21	Explorer	3 Aug 2003	−0.07	−0.07	0.16	0.16
22	Explorer	8 Aug 2003	−0.33	−0.28	0.35	0.41
23	Explorer	5 Oct 2003	−0.28	−0.21	0.65	0.56
24	Explorer	12 Oct 2003	−0.35	−0.23	0.64	0.43
25	Explorer	19 Oct 2003	−0.03	−0.03	0.16	0.15
26	Explorer	23 Oct 2003	−0.11	−0.08	0.28	0.25
27	Explorer	8 Feb 2004	−0.03	0.05	0.34	0.22
28	Explorer	29 May 2004	−0.09	−0.18	0.45	0.38
29	Explorer	16 Aug 2004	−0.07	−0.06	0.47	0.37
30	Explorer	20 Sep 2004	−0.04	0.02	0.33	0.39
31	Explorer	28 Sep 2004	−0.21	−0.18	0.45	0.33
32	Explorer	22 Oct 2004	0.03	0.06	0.26	0.23
33	Explorer	23 May 2005	−0.29	−0.11	0.83	0.57
34	Explorer	28 May 2005	−0.06	−0.06	0.34	0.25
35	Explorer	25 Jun 2005	−0.32	−0.30	0.38	0.42
36	Explorer	25 Jul 2005	−0.01	−0.02	0.26	0.18
37	Explorer	1 Aug 2005	0.15	0.11	0.20	0.18
38	Explorer	6 Aug 2005	0.19	0.16	0.23	0.17
39	Explorer	12 Aug 2005	0.31	0.54	0.62	0.64
40	Explorer	20 Aug 2005	0.02	−0.01	0.20	0.18
41	Ewing	1 Sep 2001	−0.08	−0.12	0.17	0.16
42	Ewing	8 Sep 2001	−0.09	−0.10	0.56	0.45
43	Ewing	9 Sep 2001	0.11	0.02	0.21	0.14
44	Ewing	18 Sep 2001	0.08	0.04	0.08	0.06
45	Ewing	11 Oct 2001	0.17	0.12	0.09	0.07
46	Ewing	8 Nov 2001	−0.03	−0.03	0.17	0.11
47	Ewing	9 Nov 2001	0.09	0.01	0.17	0.13
48	Ewing	10 Nov 2001	−0.30	−0.30	0.60	0.41
49	Ewing	11 Nov 2001	−0.24	−0.29	0.63	0.45
50	Ewing	13 Nov 2001	−0.31	−0.38	0.82	0.47
51	Ewing	14 Nov 2001	0.20	0.07	0.31	0.23
52	Ewing	15 Nov 2001	−0.23	−0.21	0.54	0.43
53	Ewing	17 Nov 2001	0.08	0.04	0.10	0.08
54	Revelle	30 Sep 1997	0.00	−0.01	0.05	0.05
55	Revelle	1 Oct 1997	0.02	0.00	0.06	0.06
56	Revelle	2 Oct 1997	0.33	0.32	0.35	0.74
57	Revelle	9 Oct 1997	−0.28	−0.29	0.29	0.26
58	Melville	2 Oct 1999	0.16	0.10	0.21	0.17
59	Melville	3 Oct 1999	0.12	0.01	0.23	0.15
60	Melville	5 Oct 1999	0.24	0.18	0.32	0.36
61	Melville	6 Oct 1999	0.32	0.35	0.38	0.53
62	Melville	9 Oct 1999	0.19	0.14	0.15	0.16
63	Melville	10 Oct 1999	0.63	0.65	0.70	0.85
64	Melville	11 Oct 1999	0.42	0.33	0.31	0.38
65	Melville	12 Oct 1999	−0.09	−0.16	0.69	0.53
66	Melville	13 Oct 1999	0.19	0.42	1.46	1.05
67	Melville	14 Oct 1999	−0.14	0.35	0.94	0.62
68	Melville	17 Oct 1999	0.02	0.01	0.10	0.07
69	Melville	18 Oct 1999	0.17	0.11	0.21	0.29
70	Aurora	11 Sep 2003	−0.05	−0.05	0.11	0.11
71	Aurora	13 Sep 2003	−0.06	−0.01	0.12	0.11
72	Aurora	14 Sep 2003	−0.03	−0.03	0.09	0.09

[a]STD, salinity-temperature-depth profiler.

warming, some of which are discussed here. The model was forced using measurements from the research vessels, as described by *Gentemann* [2007], to determine warming amplitude at a specified depth (the surface is used here), the vertical profile of temperature, and the depth of the warm layer. Figures 12–17 (showing individual daily time series) all have the same format. Figures 12a, 13a, 14a, 15a, 16a, and 17a have insolation in the background, wind speed (green line, axis on the right), diurnal warming (blue line, axis is on the left), F96 simulations (gray line), and POSH simulations (black line). In Figures 12b, 13b, 14b, 15b, 16b, and 17b, profiles of the temperature through the diurnal thermocline, calculated by the POSH model, are shown. For visualization purposes, the profile amplitude was normalized by the surface warming value and then scaled by the time step. Therefore, the amplitude should be taken from Figures 12a, 13a, 14a, 15a, 16a, and 17a, but the shape and depth of warming are correctly shown in Figures 12b, 13b, 14b, 15b, 16b, and 17b. Before sunrise and after the diurnal thermocline has been eroded, the temperature is constant with depth. Once a diurnal thermocline forms, the temperature profiles in Figures 12–17 end at the base of the warm layer. All 72 days were examined closely, initially to determine where the F96 model succeeded and failed in modeling observed warming. For all selected 72 days of diurnal warming in the measurement data set, the bias and standard deviation of the difference, modeled minus observed warming, from 0600 LMT onward are given in Table 2. These results lead us to the refinements implemented in the POSH model. The remainder of this section discusses 6 days with different expressions of diurnal warming and the corresponding model simulations.

[39] In Figure 12, an example is shown where there were two peaks in diurnal warming directly related to two decreases in wind speed. The warming peaks occurred slightly after the local minima in winds speed. The F96 model amplitudes were too low and temporally lag the observed peaks for both occurrences. Both peaks were well defined in the POSH simulation and the temperature maxima were close to those measured. The POSH simulations indicate the warm layer was initially very shallow, deepening with the increase in wind speed, and then decreasing in depth again as the wind decreased producing the second peak in surface temperature. The vertical temperature gradients in the diurnal thermocline were very large at low wind speeds and decreased with increasing wind speed. From 1400 to 1500 LMT the wind speed was decreasing and the profile temperature gradient increased.

[40] Diurnal warming from 3 June 2002 (Figure 13) was variable, with two local maxima, the late afternoon peak being larger than the morning peak. Variable cloud cover was present throughout the day, strongly modulating the surface insolation. The warming simulated by the F96 model underestimated the magnitude of the first temperature

Table 3. Evaluation of Model Performance for All Data Through Comparisons to 72 Days With Measured Diurnal Warming[a]

	Mean (K)	STD (K)	Number of Observations
F96	−0.02	0.35	7631
POSH	−0.01	0.28	7631

[a]The mean and standard deviation of the difference, simulated minus measured warming.

peak, placing it after the measured maximum, and then the warming in the late afternoon was too prolonged. The POSH model matched much better the timing and amplitudes of the two observed peaks. The warm layer remained relatively shallow and the simulated vertical temperature gradients were strong from 0900 to 1100 LMT, when the wind speed was low. As the wind increased from 1100 to 1230 LMT, the POSH model indicates a deepening of the diurnal thermocline and a decrease in the temperature gradients. From 1230 to 1700 LMT the wind decreased, the model shows the warm layer has thinned, and gradients increased. Finally, after 1700 LMT, the wind increased, and the model indicates the warm layer deepened and gradients decreased until the thermocline was ultimately erased after 2000 LMT.

[41] Clear skies and low wind speeds occurred on 12 July 2002 (Figure 14). The relatively constant, low wind speeds from early in the day through 1200 LMT resulted in diurnal warming that closely echoed the slope of the increasing insolation. After 1200 LMT, the winds slowly increased, decreasing the surface temperature. The F96-simulated warming was too small, occurred after the observed peak, and persisted late into the evening, long after the measured warming had become negligible. The POSH model accurately simulates the observed warming until 1230 LMT. The POSH model lagged the peak in warming by approximately 1 h and then retained too much heat in the afternoon. Warming persisted in the POSH model until 1900; approximately 2 h after observed warming had disappeared.

[42] On 13 February 2003 (Figure 15) a midafternoon increase in wind speed from 1400 to 1530 LMT rapidly erased observed warming. The wind decreased for a short period at around 1545 LMT, but radiative fluxes were small and the observed warming increased only slightly. Neither model simulation has the correct peak amplitude. The F96 model had about 50% less warming than observed, did not correctly resolve the peak, and did not diminish as quickly as the observed temperature. The POSH model followed the observed warming more closely, but it had too much warming around 1100 LMT and then, although it did resolve the peak, not enough warming was simulated. There is larger variability in POSH than either the observations or F95, likely because of the increased responsiveness to changes in insolation. The POSH model closely followed the observed temperature decrease. The low wind speeds result in very shallow and strong gradients of temperature in the warm layer predicted by the POSH model that rapidly deepened and weakened with the increase in wind speed simultaneous with a decrease in insolation at approximately 1400 LMT.

[43] A large peak in observed warming, followed by a sharp decrease was measured on 15 November 2001 from the Lamont-Doherty Earth Observatory (LDEO) R/V *Ewing* in the Indian Ocean (Figure 16). Neither of the models was able to accurately mimic the amplitude of the diurnal peak. The observed warming decreased within 10 min of the increase in wind speed and the POSH model simulations rapidly diminished alongside the data. The POSH amplitude was larger than that of F96, better matching the observed warming. After the increase in wind speed, there was no observable warming after approximately 1700 LMT, but the F96 model had warming persisting to almost 2000 LMT. The thermocline depth simulated by the POSH model increased rapidly after the increase in wind speed.

[44] Another large diurnal warming event with two peaks occurred on 11 November 2001, also in the Indian Ocean (Figure 17). Low wind speeds persisted through most of the day, increasing slightly after 1300 LMT, and small fluctuations in wind speed resulted in the two measured temperature maxima. The F96 model does not resolve the two diurnal peaks, the amplitude is less than that observed, and after a small increase in wind speed at 1600 LMT, the simulated warming is larger than observed until 2400 LMT. The POSH model closely followed the observed warming, resolving both peaks, and diminished in amplitude realistically. The low wind speeds and high insolation resulted in a very shallow diurnal thermocline with a strong gradient in temperature.

[45] Figures 12–17 are indicative of the results seen by examining all 72 days of warming. The F96 model consistently underestimated the magnitude of the warming, did not respond rapidly enough to changes in momentum and radiative fluxes, and often had more warming than observed late into the evening. This behavior may be more accurate for diurnal warming at depth rather than at the surface. The POSH model was specifically developed to model surface warming and throughout these studies it usually simulates the diurnal amplitudes and variability at the surface more accurately than the F96 model (Table 2). Table 3 shows the bias and standard deviation of the F96- and POSH-modeled warming minus the observed warming for all 72 days. Biases are approximately equal, −0.02 K and −0.01 K for F96 and POSH, respectively. The standard deviation shows the improvement in modeling accuracy with POSH (0.28 K) less than the F96 (0.35 K) error, a reduction of 20%. The low bias in the F96 simulations is the result of consistent underestimation of the temperature maxima, which contributes a negative component to the bias estimate, and overestimation of the persistence of the heating, contributing a positive component to the estimate of bias error. This is shown in Figure 18 where the bias and standard deviation are plotted for each LMT hour, with data given in Table 4. The POSH bias is always equal to or less than the F96 bias error. The F96 bias is negative (the model underestimates warming) prior to 1500. After 1500, the F96 bias is positive (the model overestimates warming). The standard deviation error for POSH is less than F96 for all hourly comparisons except prior to 1100.

4. Conclusions

[46] A surface diurnal warming model is vital since it is the upper ocean surface which is in direct contact with the atmosphere, improved determination of diurnal warming,

Table 4. Evaluation of Model Performance as a Function of LMT

	Mean (K)		STD (K)	
LMT	F96	POSH	F96	POSH
6	−0.01	−0.01	0.11	0.11
7	−0.02	−0.01	0.13	0.14
8	−0.04	−0.01	0.14	0.14
9	−0.05	0.05	0.17	0.22
10	−0.11	0.08	0.32	0.33
11	−0.25	0.03	0.50	0.45
12	−0.42	−0.11	0.66	0.58
13	−0.30	0.01	0.66	0.64
14	−0.21	−0.02	0.68	0.59
15	−0.04	−0.01	0.63	0.56
16	0.07	−0.02	0.58	0.52
17	0.13	−0.04	0.46	0.37
18	0.18	−0.03	0.38	0.33
19	0.20	−0.03	0.31	0.27
20	0.13	−0.06	0.27	0.25
21	0.14	−0.03	0.26	0.23
22	0.12	−0.04	0.25	0.22
23	0.10	−0.03	0.25	0.24
24	0.11	0.00	0.22	0.16

will lead to better estimates of air-sea heat and gas fluxes [*Ward et al.*, 2004a; *Ward and Donelan*, 2006]. Failing to account for a diurnal cycle in SSTs leads to errors in determining surface fluxes for NWP and climate models [*Kennedy et al.*, 2007; *Webster et al.*, 1996; *Woods et al.*, 1984]. Tropical atmospheric circulation is sensitive to relatively small changes in SSTs [*Palmer and Mansfield*, 1984; *Shukla*, 1998] as is local atmospheric convection [*Chen and Houze*, 1997] and SST variability in this region is important to understanding climate change.

[47] Observations of diurnal warming at the ocean surface are only available from a small number of instruments. The M-AERI deployment on the *Explorer of the Seas* provided routine measurements of skin SST temperatures in the Caribbean Sea. Data have been accumulated between 2000 and 2007 and form a significant data set of meteorological and oceanographic measurements. Data from four additional research cruises with M-AERI measurements of skin SST in the Indian Ocean, Southern Ocean, Pacific Ocean, and Gulf of California were utilized to determine the mean characteristics of diurnal warming (Figure 3). This is a unique data set of skin SST measurements with the appropriate ancillary meteorological and oceanographic parameters necessary to investigate diurnal warming variability and model skill at predicting diurnal temperature signals. These data were utilized to develop a new model of diurnal variability.

[48] The F96 model was refined to improve its performance when compared to the surface measurements of diurnal warming from M-AERI. Parameterization of the absorption of solar radiation was improved by using a nine-band spectral model with absorption increased by 20%. This change, combined with a reduction of accumulated heat and momentum, increased the model's responsiveness to changes in surface heat flux and surface stress. Wind speed–dependent, nondimensional, vertical warming profiles were added to the model. The profiles scale by the modeled heat content and warm layer thickness. At low wind speeds warming is concentrated near the surface. As wind speed increases and correspondingly the surface layer turbulent mixing increases, the temperature profiles relax to a more vertical state expected of a more mixed diurnal warm layer. These profiles are predicted at each time step in the model and provide an estimate of the vertical temperature structure within the diurnal thermocline.

[49] The POSH model appreciably increases the skill of its heritage model (F96) at simulating diurnal warming at the ocean surface. To understand intraday variability, to estimate the heat available at the surface throughout the day, and to model diurnal warming for a wide variety of applications, the POSH model has the least error when compared to the M-AERI surface measurements of diurnal warming. The use of both day and nighttime satellite SSTs in analyses requires modeling of diurnal variability. While empirical models developed specifically for satellite data sets exist, they do not provide information on the vertical structure of the upper ocean. The POSH model provides a method for determining global patterns of diurnal warming and the vertical structure of the warming. These estimates of diurnal warming at the surface could be used to determine the daily foundation temperature, defined as the temperature free of diurnal variability [*Donlon et al.*, 2007], from satellite SSTs taken at various local times, while the profiles of warming could be incorporated into ocean state and ocean forecasting models.

Appendix A: Previous Measurements of the Diurnal Temperature Profile

[50] A number of research cruises have studied how temperature changes with depth in diurnal thermoclines. This section discusses several of these studies. On of the oldest studies was in 1972, when, over 12 days, during the Barbados Oceanographic and Meteorological Experiment (BOMEX), *Delnore* [1972] acquired temperature and salinity profiles in the upper 50 m of the ocean. Five ships, each carrying an Eppley pyranometer to measure surface insolation were stationed near Barbados making over 300 profiles of the upper ocean with Bissett Berman salinity-temperature-depth profilers. Each day, profiles were taken at the same time. Surface winds were reported as 5.0–7.5 m s^{-1} for the first few days (20–26 June 1969) and increased afterward, eroding any diurnal warming. These first 6 days were used to examine the depth dependence of diurnal variability. Figure 19 shows the average temperature profile measured from the National Oceanic Atmospheric Administration (NOAA) Ship *Discoverer* over all 6 days at the various profile observation times. The formation of a warm layer of ~0.6 K with a thickness of 18 m is present by 1100 local mean time (LMT) and a more stratified, warmer layer of ~1.6 K that then linearly decreases in temperature with depth to ~20 m develops by 1400 LMT (Figure 19a). As the surface cools, the profiles at 1700 LMT are well mixed with a warm layer of approximately 1.1 K and a thickness of approximately 20 m. Thereafter, profiles slowly relax to the original mixed layer temperature. In Figure 19b the observed warming is always "well mixed" within the warm layer and the linear gradient seen at 1400 LMT in Figure 19a does not occur, likely because of the higher wind speeds during this observation period. Data from the NOAA R/V *Oceanographer* are shown in Figure 20. In Figure 20a, the warm layer is still well mixed above ~10 m, but becomes

Table A1. Definition of Symbols

Symbol	Definition	Value	Units
$T(z)$	Temperature profile in upper ocean		K
$T_c\ (z)$	Cool skin profile		K
$\Delta T_{\mathrm{dw}}\ (z)$	Diurnal warming profile		K
T_{depth}	Bulk or mixed layer temperature		K
$T(0)$	Temperature at the air-sea interface		K
T_{skin}	Temperature at the top of the skin layer		K
T_w	F96 diurnal heating at surface		K
D_T	Depth of diurnal warm layer		m
τ_{ac}	Integrated wind stress		N m^{-2}
u_*	Friction velocity		m s^{-1}
u	Wind speed at 10 m		m s^{-1}
T_a	Air temperature at 10 m		K
ρ	Density		kg m^{-3}
ρ_a	Density of air		kg m^{-3}
Q_{ac}	Integrated radiative fluxes		W m^{-2}
Q_{rain}	Heat flux due to rain		W m^{-2}
Q_{lat}	Latent heat flux		W m^{-2}
Q_{sens}	Sensible heat flux		W m^{-2}
Q_{SW}	Net shortwave radiation		W m^{-2}
Q_{LW}	Net longwave radiation		W m^{-2}
$Q_{\mathrm{LW}\downarrow}$	Downwelling longwave radiation		W m^{-2}
$Q_{\mathrm{SW}\downarrow}$	Downwelling shortwave radiation		W m^{-2}
Δt	Time step		s
θ	Solar angle		deg
c_p	Specific heat at constant pressure	1004	J kg^{-1} K^{-1}
g	Gravitational acceleration	9.72	m s^{-2}
σ_{SB}	Stephen-Boltzman constant	5.67×10^{-8}	W m^{-2} K^{-4}
r_{SW}	Mean reflectivity for shortwave radiation	0.055	
$\varepsilon_{\mathrm{LW}}$	Mean emissivity longwave radiation	0.97	
R_i	Bulk Richardson number	0.65	
f_w	Attenuation of shortwave radiation		
α	Thermal expansion coefficient		
C_H	Stanton number		
C_E	Dalton number		
q_s	Saturation specific humidity at the surface		
q_a	Saturation specific humidity at 10 m		
ε_τ	Reduction of surface momentum		
ε_χ	Reduction of heat		
a	Coefficient		

shallower and warmer throughout the day. By contrast, the measurements shown in Figure 20b had a warm layer well mixed down to 18 m. While *Delnore*'s [1972] analysis was mainly concerned with calculating the heat content and evaporation rates, these early profiles of diurnal warming point toward a family of curves for the growth and decay of warming within the mixed layer that is likely dependent on the history of radiative heating and turbulent mixing either through stress or shear-induced instabilities.

[51] More recently, the vertical distribution of diurnal heating in the upper ocean was examined using Tropical Ocean Global Atmosphere Coupled Ocean Atmosphere Response Experiment (TOGA COARE) profiles [*Soloviev and Lukas*, 1997]. Thirty-five profiles were taken and it was found that often at low wind speeds, the large diurnal signals were trapped in the top 1 m of the ocean, and at very low wind speeds confined to the upper 10 cm.

[52] Profiles shown by *Soloviev and Lukas* [1997] (Figure 21) have three distinctive vertical distributions of warming. Profiles taken at wind speeds greater than 7.0 m s^{-1} are well mixed, with diurnal warming less than 0.2 K with a warm layer depth of 12–17 m. The ten profiles taken during wind speeds of ~2.0 m s^{-1} have an almost constant warming (0.6–0.8 K) down to slightly different depths (1–7 m), a decrease in the mixed layer temperature, and then constant (mixed layer) temperature below the warm layer. As pointed out in that paper, these profiles all have almost the same amount of warming at the surface, but the warming extends to very different depths. The five profiles taken in calm weather (winds less than 2.0 m s^{-1}) have warming confined to the upper meter and a very large surface temperature increase of 3.0 K. These profiles appear to have an exponential decrease in temperature with depth.

[53] During TOGA COARE upper ocean profiles of temperature were taken from the Commonwealth Scientific and Industrial Research Organization (CSIRO) R/V *Franklin* [*Webster et al.*, 1996]. Figure 22 shows the profiles taken on 2 different days. Figure 22a shows profiles from 13 January 1993, 1 day with strong insolation and light winds that result in a diurnal warm layer of approximately 2.0 K at the surface, diminishing exponentially with depth. Figure 22b shows profiles on 4 February 1 day with strong winds and weak insolation, resulting in a well-mixed upper layer with no surface expression of diurnal warming. In Figure 22a, the base of the diurnal layer appears to be at about 2 m depth.

[54] Further profiles of diurnal warming [*Halpern and Reed*, 1976] were taken off the Northwest African coast during 24–26 March 1974 during a period of very light winds (approximately 2 m s^{-1}). Measurements of incident shortwave radiation, air temperature, humidity, and wind speed were taken from the National Oceanic Atmospheric Administration (NOAA) Ship *Oceanographer*. A buoy was fitted with 10 thermistors within the upper 24 m of the ocean. Hourly averages of the thermistors show the diurnal temperature range (Figure 23); diurnal amplitudes of 0.9 K to 1.4 K were found during the 3 days of the experiment and an exponential decrease in temperature with depth was observed (note the logarithmic scale in temperature).

[55] These measurements all show that the temperature profile, in a diurnal thermocline, is related to wind speed, and has an exponential decrease in temperature with depth. This work motivated the POSH model development to include a more realistic temperature profile. Symbols used in the paper are defined in Table A1.

[56] **Acknowledgments.** We would like to acknowledge the benefit derived from discussions with Nick Shay, Ian Robinson, Bob Evans, and Eric Chassignet. The data for this study were collected by Eddie Kearns and Bob Evans (R/V *Melville*), Chip Maxwell and Don Cucchiara (*Explorer of the Seas*), and Erica Key (R/V *Ewing* and R/V *Aurora Australis*). This work was supported by funding from NOAA (NA030AR4310126) and NASA (NM0710772, NAG5–11104, NNG04HZ33C, NNG04GM56G, and NAS5–31361). This paper is based in part upon work supported by the National Science Foundation under grant 0525657. Two anonymous reviewers are thanked for their thoughtful suggestions.

References

Anderson, S. P., R. A. Weller, and R. B. Lukas (1996), Surface buoyancy forcing and the mixed layer of the western Pacific warm pool: Observations and 1D model results, *J. Clim.*, *9*(12), 3056–3086, doi:10.1175/1520-0442(1996)009<3056:SBFATM>2.0.CO;2.

Böhm, E., S. Marullo, and R. Santoleri (1991), AVHRR visible-IR detection of diurnal warming events in the western Mediterranean Sea, *Int. J. Remote Sens.*, *12*, 695–701, doi:10.1080/01431169108929686.

Chen, S. S., and R. A. Houze (1997), Diurnal variation and life-cycle of deep convective systems over the tropical Pacific warm pool, *Q. J. R. Meteorol. Soc.*, *123*, 357–388, doi:10.1002/qj.49712353806.

Cornillon, P., and L. Stramma (1985), The distribution of diurnal sea surface warming events in the western Sargasso Sea, *J. Geophys. Res.*, *90*, 811–815.

Cronin, M. F., and M. J. McPhaden (1997), The upper ocean heat balance in the western equatorial Pacific warm pool during September–December 1992, *J. Geophys. Res.*, *102*, 8533–8553, doi:10.1029/97JC00020.

Defant, A. (1961), *Physical Oceanography*, Pergamon, New York.

Delnore, V. E. (1972), Diurnal variation of temperature and energy budget for the oceanic mixed layer during BOMEX, *J. Phys. Oceanogr.*, *2*, 239–247, doi:10.1175/1520-0485(1972)002<0239:DVOTAE>2.0.CO;2.

Deschamps, P. Y., and R. Frouin (1984), Large diurnal heating of the sea surface observed by the HCMR experiment, *J. Phys. Oceanogr.*, *14*, 177–185, doi:10.1175/1520-0485(1984)014<0177:LDHOTS>2.0.CO;2.

Donlon, C. J., P. J. Minnett, I. J. Barton, T. J. Nightingale, and C. L. Gentemann (2001), The character of skin and subsurface sea surface temperature, report, World Meteorol. Organ., Geneva, Switzerland.

Donlon, C. J., P. J. Minnett, C. L. Gentemann, T. J. Nightingale, I. J. Barton, B. Ward, and M. J. Murray (2002), Toward improved validation of satellite sea surface skin temperature measurements for climate research, *J. Clim.*, *15*(4), 353–369, doi:10.1175/1520-0442(2002)015<0353:TIVOSS>2.0.CO;2.

Donlon, C. J., et al. (2007), The Global Ocean Data Assimilation Experiment (GODAE) High-Resolution Sea Surface Temperature Pilot Project (GHRSST-PP), *Bull. Am. Meteorol. Soc.*, *88*(8), 1197–1213, doi:10.1175/BAMS-88-8-1197.

Fairall, C. W., E. F. Bradley, J. S. Godfrey, G. A. Wick, J. B. Edson, and G. S. Young (1996a), Cool-skin and warm-layer effects on sea surface temperature, *J. Geophys. Res.*, *101*, 1295–1308, doi:10.1029/95JC03190.

Fairall, C. W., G. S. Young, E. F. Bradley, D. P. Rogers, and J. B. Edson (1996b), Bulk parameterization of air-sea fluxes for Tropical Ocean–Global Atmosphere Coupled-Ocean Atmosphere Response Experiment, *J. Geophys. Res.*, *101*, 3747–3764, doi:10.1029/95JC03205.

Fairall, C. W., E. F. Bradley, J. E. Hare, A. A. Grachev, and J. B. Edson (2003), Bulk parameterization of air-sea fluxes: Updates and verification for the COARE algorithm, *J. Clim.*, *16*(4), 571–591, doi:10.1175/1520-0442(2003)016<0571:BPOASF>2.0.CO;2.

Gentemann, C. L. (2007), Diurnal warming at the ocean surface, Ph.D. thesis, 163 pp., Div. of Meteorol. and Phys. Oceanogr., Univ. of Miami, Miami, Fla.

Gentemann, C. L., and P. J. Minnett (2008), Radiometric measurements of ocean surface thermal variability, *J. Geophys. Res.*, *113*, C08017, doi:10.1029/2007JC004540.

Gentemann, C. L., C. J. Donlon, A. Stuart-Menteth, and F. J. Wentz (2003), Diurnal signals in satellite sea surface temperature measurements, *Geophys. Res. Lett.*, *30*(3), 1140, doi:10.1029/2002GL016291.

Halpern, D., and R. Reed (1976), Heat budget of the upper ocean under light winds, *J. Phys. Oceanogr.*, *6*, 972–976, doi:10.1175/1520-0485(1976)006<0972:HBOTUO>2.0.CO;2.

Implementation Advisory Group (1999), Global physical ocean observations for GOOS/GCOS: An action plan for existing bodies and mechanisms, *GOOS Rep. 66*, Intergov. Oceanogr. Comm., Paris.

Kantha, L. H., and C. A. Clayson (1994), An improved mixed layer model for geophysical applications, *J. Geophys. Res.*, *99*, 25,235–25,266, doi:10.1029/94JC02257.

Katsaros, K. B., A. Soloviev, R. H. Weisberg, and M. E. Luther (2005), Reduced horizontal sea surface temperature gradients under conditions of clear skies and weak winds, *Boundary Layer Meteorol.*, *116*, 175–185, doi:10.1007/s10546-004-2421-4.

Kawai, Y., and A. Wada (2007), Diurnal sea surface temperature variation and its impact on the atmosphere and ocean: A review, *J. Oceanogr.*, *63*(5), 721–744, doi:10.1007/s10872-007-0063-0.

Kennedy, J. J., P. Brohan, and S. F. B. Tett (2007), A global climatology of the diurnal variations in sea surface temperature and implications for MSU temperature trends, *Geophys. Res. Lett.*, *34*, L05712, doi:10.1029/2006GL028920.

Knuteson, R. O., et al. (2004a), Atmospheric emitted radiance interferometer. Part I: Instrument design, *J. Atmos. Oceanic Technol.*, *21*(12), 1763–1776, doi:10.1175/JTECH-1662.1.

Knuteson, R. O., et al. (2004b), Atmospheric emitted radiance interferometer. Part II: Instrument performance, *J. Atmos. Oceanic Technol.*, *21*(12), 1777–1789, doi:10.1175/JTECH-1663.1.

Mellor, G. L., and T. Yamada (1982), Development of a turbulent closure model for geophysical fluid problems, *Rev. Geophys.*, *20*, 851–875, doi:10.1029/RG020i004p00851.

Merchant, C. J., et al. (2008), Deriving a sea surface temperature record suitable for climate change research from the along-track scanning radiometers, *Adv. Space Res.*, *41*(1), 1–11, doi:10.1016/j.asr.2007.07.041.

Minnett, P. J. (2003), Radiometric measurements of the sea-surface skin temperature—The competing roles of the diurnal thermocline and the cool skin, *Int. J. Remote Sens.*, *24*, 5033–5047, doi:10.1080/0143116031000095880.

Minnett, P. J., R. O. Knuteson, F. A. Best, B. J. Osborne, J. A. Hanafin, and O. B. Brown (2001), The Marine-Atmospheric Emitted Radiance Interferometer (M-AERI), a high-accuracy, seagoing infrared spectroradiometer, *J. Atmos. Oceanic Technol.*, *18*(6), 994–1013, doi:10.1175/1520-0426(2001)018<0994:TMAERI>2.0.CO;2.

Niiler, P. P., and E. B. Kraus (1977), One-dimensional models of the upper ocean, in *Modelling and Prediction of the Upper Layers of the Ocean*, edited by E. B. Kraus, pp. 143–172, Pergamon, Oxford, U. K.

Notarstefano, G., E. Mauri, and P. M. Poulain (2006), Near-surface thermal structure and surface diurnal warming in the Adriatic Sea using satellite and drifter data, *Remote Sens. Environ.*, *101*(2), 194–211, doi:10.1016/j.rse.2005.12.013.

O'Carroll, A. G., B. Candy, and R. W. Saunders (2001), Conversion of ATSR-2 sea surface skin to bulk temperature for use in climate studies, report, U.K. Meteorol. Off., Bracknell, U.K.

O'Carroll, A. G., J. G. Watts, L. A. Horrocks, R. W. Saunders, and N. A. Rayner (2004), Influence of sea surface temperature products from the ATSR series on HadISST1 global analyses, report, U.K. Meteorol. Off., Bracknell, U.K.

Palmer, T. N., and D. A. Mansfield (1984), Response of two atmospheric general circulation models to sea-surface temperature anomalies in the tropical East and West Pacific, *Nature*, *310*(5977), 483–485, doi:10.1038/310483a0.

Paulson, C. A., and J. J. Simpson (1981), The temperature difference across the cool skin of the ocean, *J. Geophys. Res.*, *86*, 11,044–11,055, doi:10.1029/JC086iC11p11044.

Price, J. F., C. N. K. Mooers, and J. C. Van Leer (1978), Observation and simulation of storm-induced mixed-layer deepening, *J. Phys. Oceanogr.*, *8*, 582–599, doi:10.1175/1520-0485(1978)008<0582:OASOSI>2.0.CO;2.

Price, J. F., R. A. Weller, and R. Pinkel (1986), Diurnal cycling: Observations and models of the upper ocean response to diurnal heating, cooling, and wind mixing, *J. Geophys. Res.*, *91*, 8411–8427, doi:10.1029/JC091iC07p08411.

Rice, J. P., S. C. Bender, W. H. Atkins, and F. J. Lovas (2003), Deployment test of the NIST EOS thermal-infrared transfer radiometer, *Int. J. Remote Sens.*, *24*, 367–388, doi:10.1080/01431160304975.

Rice, J. P., J. J. Butler, B. C. Johnson, P. J. Minnett, K. A. Maillet, T. J. Nightingale, S. J. Hook, A. Abtahi, C. J. Donlon, and I. Barton (2004), The Miami 2001 infrared radiometer calibration and intercomparison: 1. Laboratory characterization of blackbody targets, *J. Atmos. Oceanic Technol.*, *21*(2), 258–267, doi:10.1175/1520-0426(2004)021<0258:TMIRCA>2.0.CO;2.

Schluessel, P., W. J. Emery, H. Grassl, and T. Mammen (1990), On the bulk-skin temperature difference and its impact on satellite remote sensing of sea surface temperature, *J. Geophys. Res.*, *95*, 13,341–13,356, doi:10.1029/JC095iC08p13341.

Shinoda, T., and H. Hendon (1998), Mixed layer modeling of intraseasonal variability in the tropical western Pacific and Indian oceans, *J. Clim.*, *11*(10), 2668–2685, doi:10.1175/1520-0442(1998)011<2668:MLMOIV>2.0.CO;2.

Shukla, J. (1998), Predictability in the midst of chaos: A scientific basis for climate forecasting, *Science*, *282*(5389), 728–731, doi:10.1126/science.282.5389.728.

Soloviev, A., and R. B. Lukas (1997), Observations of large diurnal warming events in the near-surface layer of the western equatorial Pacific warm pool, *Deep Sea Res., Part I*, *44*(6), 1055–1076, doi:10.1016/S0967-0637(96)00124-0.

Soloviev, A., and P. Schlüssel (1996), Evolution of cool skin and direct air-sea gas transfer coefficient during daytime, *Boundary Layer Meteorol.*, *77*, 45–68, doi:10.1007/BF00121858.

Stuart-Menteth, A., I. S. Robinson, R. A. Weller, and C. J. Donlon (2005), Sensitivity of the diurnal warm layer to meteorological fluctuations Part 1: Observations, *J. Atmos. Ocean Sci.*, *10*(3), 193–208, doi:10.1080/17417530500529521.

Sverdrup, H. U., M. W. Johnson, and R. H. Fleming (1942), *The Oceans: Their Physics, Chemistry, and General Biology*, Prentice-Hall, Englewood Cliff, N. J.

Ward, B. (2006), Near-surface ocean temperature, *J. Geophys. Res.*, *111*, C02004, doi:10.1029/2004JC002689.

Ward, B., and M. A. Donelan (2006), Thermometric measurements of the molecular sublayer at the air-water interface, *Geophys. Res. Lett.*, *33*, L07605, doi:10.1029/2005GL024769.

Ward, B., R. Wanninkhof, W. R. McGillis, A. T. Jessup, M. D. DeGrandpre, J. E. Hare, and J. B. Edson (2004a), Biases in the air-sea flux of CO_2 resulting from ocean surface temperature gradients, *J. Geophys. Res.*, *109*, C08S08, doi:10.1029/2003JC001800.

Ward, B., R. Wanninkhof, P. J. Minnett, and M. J. Head (2004b), SkinDeEP: A profiling instrument for upper-decameter sea surface measurements, *J. Atmos. Oceanic Technol.*, *21*(2), 207–223, doi:10.1175/1520-0426(2004)021<0207:SAPIFU>2.0.CO;2.

Webster, P. J., C. A. Clayson, and J. A. Curry (1996), Clouds, radiation, and the diurnal cycle of sea surface temperature in the tropical western Pacific, *J. Clim.*, *9*(8), 1712–1730, doi:10.1175/1520-0442(1996)009<1712:CRATDC>2.0.CO;2.

Weller, R. A., and S. P. Anderson (1996), Surface meteorology and air-sea fluxes in the western equatorial Pacific warm pool during the TOGA Coupled Ocean-Atmosphere Response Experiment, *J. Clim.*, *9*(8), 1959–1990, doi:10.1175/1520-0442(1996)009<1959:SMAASF>2.0.CO;2.

Wick, G. A., J. J. Bates, and D. J. Scott (2002), Satellite and skin-layer effects on the accuracy of sea surface temperature measurements from the GOES satellites, *J. Atmos. Oceanic Technol.*, *19*(11), 1834–1849, doi:10.1175/1520-0426(2002)019<1834:SASLEO>2.0.CO;2.

Woods, J. D., and W. Barkmann (1986), The response of the upper ocean to solar heating. I: The mixed layer, *Q. J. R. Meteorol. Soc.*, *112*, 1–27, doi:10.1002/qj.49711247102.

Woods, J. D., W. Barkmann, and A. Horch (1984), Solar heating of the oceans — Diurnal, seasonal, and meridional variations, *Q. J. R. Meteorol. Soc.*, *110*, 633–686.

Yokoyama, R., S. Tanba, and T. Souma (1995), Sea surface effects on the sea surface temperature estimation by remote sensing, *Int. J. Remote Sens.*, *16*, 227–238, doi:10.1080/01431169508954392.

C. L. Gentemann, Remote Sensing Systems, Suite 200, 438 First Street, Santa Rosa, CA 95401, USA. (gentemann@remss.com)

P. J. Minnett, Rosenstiel School of Marine and Atmospheric Science, University of Miami, 4600 Rickenbacker Causeway, Miami, FL 33149, USA. (pminnett@rsmas.miami.edu)

B. Ward, School of Physics, National University of Ireland, Galway 23508, Ireland. (bward@nuigalway.ie)